Structure and Dynamics of the HIV-1 Vpu Transmembrane Domain Revealed by Solid-State NMR with Magic-Angle Spinning†

Simon Sharpe, Wai-Ming Yau, and Robert Tycko*

Laboratory of Chemical Physics, National Institutes of Diabetes and Digestive and Kidney Disease, National Institutes of Health, Bethesda, Maryland 20892-0520

Received September 1, 2005; Revised Manuscript Received November 17, 2005

ABSTRACT: We report solid-state nuclear magnetic resonance (NMR) measurements on the peptide Vpu(1−40), comprising residues 1−40 of the 81-residue type 1 integral membrane protein Vpu encoded by the HIV-1 genome. On the basis of a combination of ^{13}C and ^{15}N NMR chemical shifts under magic-angle spinning (MAS), effects of local mobility on NMR signal intensities, site-specific MAS NMR line widths, and NMR-detected hydrogen−deuterium exchange, we develop a model for the structure and dynamics of the Vpu(1−40) monomer in phospholipid bilayer membranes. Our data are largely consistent with earlier structural studies of Vpu peptides by Opella and co-workers, in which solution NMR and solid-state NMR without MAS were used, but our data provide new information about local variations in the degree of mobility and structural order. In addition, our data indicate that the transmembrane α-helix of Vpu(1−40) extends beyond the hydrophobic core of the bilayer. We find no evidence for heterogeneity in the conformation and intermolecular contacts of the transmembrane α-helix, with the exception of two distinct chemical shifts observed for the Cα and Cβ atoms of A18 that may reflect distinct modes of helix−helix interaction. These results have possible implications for the supramolecular structure of Vpu oligomers that form cation-selective ion channels.

Vpu is an 81-amino acid integral membrane protein encoded by the HIV-1 genome (*1*, *2*). An accessory protein, Vpu has not been observed in virus particles, but is expressed in the host $CD4^+$ cells and localized to the rough endoplasmic reticulum (ER) and the plasma membrane. Several lines of evidence indicate that Vpu plays two distinct roles in the viral life cycle, correlated with two distinct protein domains (*3*, *4*). The N-terminal transmembrane (TM)[1] domain of Vpu has been shown to form homooligomers both in vivo and in vitro (*5*). Oligomeric Vpu has a cation-specific ion channel activity for which only the TM sequence is required (*6*, *7*). The presence of an active Vpu TM domain is required for the enhanced release of mature virus particles from the cell surface (*2*, *8*−*10*). This may be a direct consequence of the channel activity or, as recently suggested by a number of groups (*11*, *12*), may be a consequence of interactions of the Vpu TM domain with other factors present at the host cell surface, such as the TASK-1 K^+ channel. Studies of mutant and truncated Vpu proteins have shown that a TM domain with the correct amino acid sequence is sufficient and required for this activity (*13*−*15*).

The second role of Vpu is to mediate the degradation of the CD4 receptor in the ER (*16*−*19*). This role is believed to depend on interactions of the cytoplasmic domain with both the cytoplasmic tail of CD4 (*20*−*22*) and the β-transducin-repeat-containing protein (βTrCP) component of the $SCF^{\beta TrCP}$ E3 ubiquitin ligase complex (*23*) (reviewed in ref *24*). Analysis of mutant Vpu sequences indicates that the majority of the Vpu TM domain is not required for this activity, although mutations within the C-terminal portion (I20−W22) eliminate CD4 binding (*15*). It has been demonstrated that elements of the Vpu cytoplasmic domain are necessary for CD4 binding, although the precise sequence requirements are not clearly defined (*24*). A recent solution nuclear magnetic resonance (NMR) study of Vpu(41−62) [where Vpu(X−Y) indicates residues X−Y of the full-length Vpu sequence] bound to βTrCP shows close association of the phosphorylated S52 and S56 residues with the ubiquitin ligase complex (*25*).

Analysis of the available Vpu sequences from group M isolates of HIV-1 has revealed a surprising degree of sequence conservation within the TM domain, including several aliphatic residues (V9−V13, I17, and I24), W22, S23, and an EYRK motif in the C-terminal juxtamembrane region (*26*). The extreme N-terminal residues (M1−I6) vary sig-

† This work was supported in part by the Intramural Research Program of the National Institutes of Health (NIH), the National Institute of Diabetes and Digestive and Kidney Diseases (NIDDK), and the Intramural AIDS Targeted Antiviral Program (IATAP) of the NIH. S.S. was supported by a fellowship from the Canadian Institutes of Health Research.

* To whom correspondence should be addressed: National Institutes of Health, Building 5, Room 112, Bethesda, MD 20892-0520. Phone: (301) 402-8272. Fax: (301) 496-0825. E-mail: robertty@mail.nih.gov.

[1] Abbreviations: CD, circular dichroism; CP, cross-polarization; CSA, chemical shift anisotropy; DMPC, 1,2-dimyristoyl-3-*sn*-phosphatidylcholine; DOPC, 1,2-dioleoyl-3-*sn*-phosphatidylcholine; DOPG, 1,2-dioleoyl-3-*sn*-phosphatidylglycerol; DP, direct polarization; FTIR, Fourier transform infrared; MAS, magic-angle spinning; MLV, multilamellar vesicle; NMR, nuclear magnetic resonance; PAGE, polyacrylamide gel electrophoresis; RAD, radio frequency-assisted diffusion; rf, radio frequency; SDS, sodium dodecyl sulfate; SPECIFIC−CP, spectrally induced filtering in combination with cross-polarization; TFE, 2,2,2-trifluoroethanol; TM, transmembrane; TPPM, two-pulse phase-modulated.

10.1021/bi051766k
Published on Web 12/23/2005

nificantly among viral strains. A detailed understanding of the structure and dynamical behavior of the TM domain will likely provide insight into the functional role this protein plays in the HIV-1 life cycle.

To date, structural studies of Vpu and various fragments of Vpu have employed a number of experimental techniques. Circular dichroism measurements on Vpu(1−39) indicate that this peptide contains 55% α-helical structure in 2,2,2-trifluoroethanol/H_2O (TFE/H_2O) solutions (*27*). Similar measurements on a series of overlapping peptides from Vpu(28−42) to Vpu(67−81) showed significant helical content for residues 42−50 and 57−69 (*28*). Fourier transform infrared (FTIR) dichroism spectroscopy of Vpu(1−31) in DMPC bilayers suggests that this peptide is predominantly α-helical in nature (*29*). Solution NMR of Vpu(32−81) in TFE/H_2O solutions indicates helical structure for residues 37−51 and 57−72 (*28*, *30*). Similar studies performed in the absence of TFE, but in the presence of high salt concentrations, show helical regions spanning residues 40−50, 60−68, and 75−79 (*31*). A dependence of the cytoplasmic domain structure on phosphorylation of S52 and S56 has been shown by NMR studies of Vpu(41−62) in an aqueous solvent (*25*, *32*). Solution NMR studies of Vpu peptides in the presence of DHPC micelles show evidence of helical regions from residues 5−30 in Vpu(2−37) (*33*), 8−25 in Vpu(2−30) (*34*), and 28−50 and 58−70 in Vpu(28−81) (*33*). Solid-state NMR measurements on Vpu peptides of various lengths incorporated into oriented lipid bilayers have been used to demonstrate that the majority of residues within Vpu(2−37) lie within helical regions oriented approximately perpendicular to the bilayer surface, while most residues of Vpu(28−81) give solid-state NMR spectra which are inconsistent with such an orientation (*4*, *33*). More recently, Park et al. have determined the backbone structure of an α-helix spanning residues 8−25 of a modified Vpu(2−30) peptide by solid-state NMR in oriented bilayers (*34*). In addition to these experimental studies, several groups have used molecular dynamics simulations and energy minimization to obtain models of both the monomeric Vpu TM domain (*35*−*37*) and the putative pore structure (*38*−*42*) (reviewed in refs *43* and *44*), including a recent model based on the monomer backbone structure of residues 8−25 (*34*).

The consensus that emerges from these earlier experimental and simulation studies is that full-length Vpu adopts a structure in bilayers in which the TM helical segment lies between residues 5−8 and 25−30, with a helical tilt of 6−15° relative to the bilayer normal (in DOPC/DOPG bilayers), although this value is strongly dependent on the hydrophobic thickness of the membrane and the method used to measure the tilt (*29*, *34*, *45*). The cytoplasmic domain consists of an amphipathic helix (from residues 30−40 to 50), most likely in the plane of the bilayers, linked to a C-terminal helix (residues 60−70, approximately) whose orientation relative to the bilayer surface is less certain.

In this paper, we report solid-state NMR measurements on Vpu(1−40) in phospholipid bilayers that provide new constraints on the structure and dynamics of the TM domain. Unlike earlier solid-state NMR studies, which employed techniques specific for oriented samples (*4*, *27*, *33*, *34*, *45*, *46*), our studies of Vpu(1−40) employ magic-angle spinning (MAS) NMR techniques and unoriented samples. As a result, the information contained in our measurements is independent and qualitatively different. In particular, we report isotropic ^{15}N and ^{13}C NMR chemical shifts for the majority of backbone and side chain sites in Vpu(1−40), which provide constraints on local conformation, ^{15}N and ^{13}C NMR line widths, which provide information about local structural order and dynamics, and hydrogen−deuterium (H−D) exchange measurements detected through two-dimensional (2D) $^{15}N-^{13}C$ solid-state NMR spectra, which provide information about solvent exposure and structural stability at a site-specific level. We also describe measurements of the dependence of solid-state NMR signal intensities and line widths on temperature and hydration level that contribute to the development of a consistent picture of the local and global dynamical behavior of Vpu(1−40) in bilayers. ^1H, ^{13}C, and ^{15}N NMR relaxation properties are also described in the context of local and global motion in Vpu(1−40). On the basis of these solid-state MAS NMR measurements, we develop a model for a single Vpu(1−40) molecule within an oligomeric bundle.

In addition to their relevance to Vpu structure and function, our results are significant in light of current interest in viroporins in general (*47*). The viroporins comprise a number of small hydrophobic viral proteins, including M2 from influenza A (*48*−*51*), the p7 protein from hepatitis C (*52*, *53*), and Vpu (*6*, *54*), among others. While detailed structural information is only available for the M2 proton channel (*55*, *56*) and Vpu (*31*, *32*, *34*), these proteins exhibit a common ability to permeabilize membranes through formation of homooligomeric ion channels or pores. Their roles in the life cycles of several pathogenic viruses make them attractive as targets for developing antiviral therapies. No crystal structure has been reported yet for any viroporin.

MATERIALS AND METHODS

Sample Preparation. Vpu(1−40) peptides, corresponding to residues 1−40 of HIV-1 Vpu, were synthesized on an Applied Biosystems 433A automated peptide synthesizer, using FMOC chemistry. Peptides were dissolved in trifluoroacetic acid and purified by reverse-phase HPLC on a semipreparative Vydac C4 column (acetonitrile/2-propanol/water gradient). Peptide identity and purity were confirmed using electrospray mass spectrometry. Vpu(1−40) peptides were synthesized with selective incorporation of U-^{13}C,^{15}N-labeled amino acids according to the following labeling schemes: $Vpu(1-40)_{AV}$ (A18, V25), $Vpu(1-40)_{PVVAIR}$ (P3, V12, V13, A14, I24, R34), $Vpu(1-40)_{ASIYRL}$ (A7, S23, I26, Y29, R30, L33), $Vpu(1-40)_{VALIEK}$ (V9, A10, L11, I27, E28, K31), $Vpu(1-40)_{IQIWK}$ (I4, Q5, I6, W22, K37), $Vpu(1-40)_{6V}$ (V9, V11, V12, V20, V21, V25), $Vpu(1-40)_{4A}$ (A7, A10, A14, A18), and $Vpu(1-40)_{8I}$ (I8, I15, I16, I17, I19, I24, I26, I27). The total sequence coverage of these labeling schemes is given in Figure 1A. 1,2-Dioleoyl-3-*sn*-phosphatidylcholine (DOPC) and 1,2-dioleoyl-3-*sn*-phosphatidylglycerol (DOPG) were obtained from Avanti Polar Lipids (Birmingham, AL).

To prepare multilamellar vesicles (MLVs) containing Vpu(1−40), dry peptide (4−6 mg) was dissolved in TFE. Any insoluble material was removed by centrifugation, and the final peptide concentration was confirmed by monitoring the UV absorbance at 278 nm. An appropriate amount of DOPC and DOPG (at a 9:1 molar ratio) was dissolved in ∼1 mL

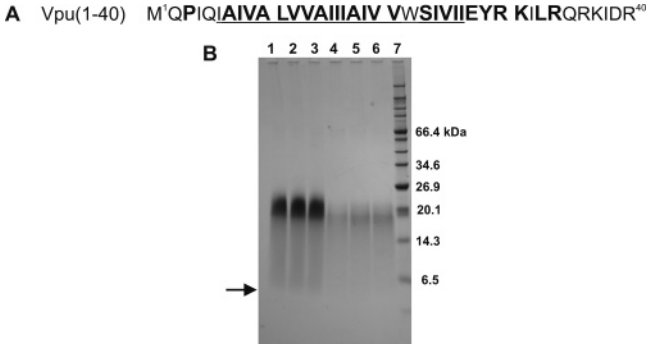

FIGURE 1: Primary structure and oligomeric state of Vpu(1−40). (A) Amino acid sequence of synthetic Vpu(1−40) peptides. The α-helical segment determined by data in this paper is underlined. Sites at which uniformly ^{13}C- and ^{15}N-labeled amino acids have been incorporated and for which NMR data are obtained are indicated in bold. (B) Coomassie blue-stained SDS−PAGE gel of several Vpu(1−40) samples at 200 (lanes 1−3) or 20 μM (lanes 4−6) peptide. Samples were heated for 10 min at 25 (lanes 1 and 4), 55 (lanes 2 and 5), or 99 °C (lanes 3 and 6) prior to loading. Molecular masses for the protein markers in lane 7 are shown at the right. The arrow indicates the expected band position for a Vpu(1−40) monomer, based on a monomer molecular mass of 4655 Da.

of $CHCl_3$, and the peptide solution was added dropwise to give a final peptide:lipid ratio of 1:33 (3 mol % peptide relative to lipids). After thorough mixing and visually apparent codissolution, the organic solvent was removed and samples were subsequently hydrated, using one of the following methods.

In the first method, the organic solvent was removed by rotary evaporation in a round-bottom flask followed by desiccation for 24 h under high vacuum. An appropriate amount (typically 50−200% of the sample dry weight) of H_2O was added to the dry protein−lipid film. The sample was then agitated in the presence of small glass beads until it was homogenized. Five freeze−thaw cycles were used to ensure even dispersion of water throughout the sample. The hydrated phospholipid bilayer preparation was then transferred to a 3.2 mm Varian MAS rotor. In the case of medium-wall rotors (22 μL volume), rotor drive tips and end caps were sealed in place with gel-formula Krazy glue to prevent sample dehydration. Thin-wall rotors (36 μL volume) were found to be self-sealing and did not require glue. Sample weight was used as an indicator of the hydration level, and did not change over the course of the NMR measurements described below.

The second method emulated protocols described for preparation of mechanically oriented lipid bilayers (*33*, *34*, *57*), and allowed lower hydration levels to be achieved in a controlled manner. In this case, hydrated samples were prepared by drying the protein/lipid solution (in TFE/$CHCl_3$) onto a clean glass slide under a stream of dry N_2(g). Residual solvent was removed from the protein−lipid film by desiccation for 24 h under vacuum. Lipid−protein bilayers were hydrated at 42 °C in a chamber kept at 93% relative humidity with a saturated solution of $(NH_4)_2PO_4$ (pH 7.0). Sample hydration was monitored by weighing, and typically achieved a maximum level of 15−20% H_2O relative to dry sample weight after 4−5 days in the hydration chamber. Once the desired hydration level was achieved, samples were packed into 3.2 mm MAS rotors for NMR experiments and sealed as described above, with care taken to avoid water loss. While accurate measurement of pH in low-water samples was difficult, sample pH was typically found to lie between 5 and 6.

SDS−PAGE Analysis of Vpu(1−40). Dry peptide was dissolved in TFE at 2 mg/mL, as described above, and the final concentration of Vpu(1−40) was calculated from the UV absorbance (278 nm) of the solution. The clarified peptide solution was divided into aliquots and dried under N_2(g). Residual solvent was removed by placing samples in a vacuum for 16 h. The 2× LDS sample buffer (Invitrogen) was added to give final peptide concentrations of 0.2 or 0.02 mM in the loading buffer. Following extensive mixing and vortexing, samples were loaded onto a 12% precast bis-tris sodium dodecyl sulfate−polyacrylamide electrophoresis (SDS−PAGE) gel (Invitrogen), which was run at 200 V for 20 min. Gels were stained with Gelcode Coomassie Blue stain (Pierce). Preincubation of samples by heating at 50, 75, or 100 °C did not affect results. Likewise, similar peptide mobility on SDS−PAGE was observed without predissolution in TFE prior to the LDS loading buffer.

Solid-State NMR. ^{13}C and ^{15}N NMR spectra were obtained on a Varian InfinityPlus-400 spectrometer (^{13}C and ^{15}N NMR frequencies of 100.4 and 40.46 MHz, respectively), using a Varian triple-resonance 3.2 mm MAS probe with a home-built variable-temperature stack to provide N_2 gas at a controlled temperature to the sample space in the probe. Additional ^{13}C NMR spectra were obtained on an Infinity-Plus-600 spectrometer (^{13}C and ^{15}N NMR frequencies of 150.6 and 60.71 MHz, respectively), using a Varian 5.0 mm MAS probe. MAS frequencies were typically 3−10 kHz, controlled to within 2 Hz. Sample temperatures under MAS were calibrated using the ^{207}Pb NMR chemical shift of solid $PbNO_3$ (*58*). NMR spectra of Vpu(1−40) in DOPC/DOPG membranes were recorded at 40 and −50 °C. The latter temperature is well below the fluid−gel phase transition of the DOPC/DOPG membranes (−20 °C) (*59*), as indicated by the broadening of ^{13}C NMR signals from the lipids at the lower temperatures. The MAS frequencies used here did not perturb the bilayer nature of the samples (as monitored by ^{31}P NMR and visual inspection), consistent with the findings of Epand et al. (*60*).

^{1}H and ^{13}C radio frequency (rf) field strengths of 50−65 kHz were typically used for cross polarization (CP) (*61*), with a ±10% amplitude ramp on the ^{13}C channel. ^{15}N NMR spectra were obtained using 40−45 and 40−60 kHz rf fields for ^{1}H and ^{15}N, respectively. ^{31}P NMR spectra were acquired with direct polarization (DP), using 50 kHz rf field strengths. Static ^{15}N and ^{31}P NMR spectra were obtained using a Hahn-echo pulse sequence with echo delay times of 100−500 μs. Two-dimensional (2D) $^{13}C-^{13}C$ NMR spectra were obtained with mixing periods of 10−25 ms using radio frequency-assisted diffusion (RAD) (*62*, *63*) recoupling. 2D $^{13}C-^{13}C$ NMR spectra were recorded with 256 t_1 points, with an increment of 38 μs. 2D $^{15}N-^{13}C$ spectra were obtained using a spectrally induced filtering in combination with a cross-polarization (SPECIFIC−CP) pulse sequence to give a frequency-selective polarization transfer from ^{15}N to $^{13}C\alpha$ following the t_1 period (*64*, *65*). A shaped CP ramp with a 3 ms contact time and average ^{13}C and ^{15}N rf fields of 7 and 2 kHz, respectively, was used to achieve the SPECIFIC−CP transfer. In H−D exchange experiments, a short (0.2 ms) $^{1}H-^{15}N$ CP contact time was used deliberately to reduce

signal contributions from nonbonded, nonexchangeable protons. 2D $^{15}N-^{13}C$ NMR spectra were recorded with 256 t_1 points, with an increment of 51 μs. Total measurement times were typically 24−48 h for 2D $^{13}C-^{13}C$ spectra and 12−20 h for 2D $^{15}N-^{13}C$ spectra. A recycle delay of 2 s was used in all cases. Two-pulse phase-modulated (TPPM) ^{1}H decoupling fields of 120 kHz were applied during the t_1 and t_2 periods (*66*).

^{15}N T_1 and T_2 spin relaxation times were measured using inversion−recovery and spin−echo pulse sequences, respectively, with rf fields as described above. Amide proton T_1 relaxation times were measured using a ^{1}H inversion−recovery sequence followed by CP to ^{15}N (0.2 ms CP period). This allowed selective detection of the amide proton relaxation behavior without the need for ^{1}H resolution. Recycle delays of 5 s were used for T_1 measurements. ^{1}H $T_{1\rho}$ relaxation times were measured from ^{13}C signal intensities using a pulse sequence in which the $^{1}H-^{13}C$ CP was preceded by a ^{1}H spin-lock period. Likewise, ^{13}C $T_{1\rho}$ relaxation times were measured using a pulse sequence in which the $^{1}H-^{13}C$ CP was followed by a ^{13}C spin-lock period.

H−D Exchange. Hydrated DOPC/DOPG MLVs containing 3 mol % Vpu(1−40) were homogenized in a 10-fold excess volume of D_2O and incubated for 1.5 h at 25 °C, punctuated with five cycles of freezing and thawing to allow full dispersion of D_2O across the lipid bilayers. Samples were then spread on clean glass slides, and bulk water was removed by evaporation under N_2(g) with manual mixing to allow uniform evaporation. Sample weight was monitored, and once the hydration level reached 17 wt %, samples were packed into 3.2 mm MAS rotors as described above and frozen for subsequent NMR analysis. The total exchange time of thawed samples was 1.75−2.0 h in each case. For each sample, one-dimensional (1D) ^{13}C, 1D ^{15}N, and 2D $^{15}N-^{13}C$ NMR spectra were obtained under identical conditions before and after exchange. The intensity of peaks in the 1D ^{13}C spectrum was used to normalize the 2D correlation spectra for total peptide content within the NMR samples. Samples were kept frozen until solid-state NMR measurements were complete. The exchange time, temperature, and pH (6−7) used for H−D exchange on Vpu(1−40) were chosen to produce >80% exchange of amide protons in a model soluble, helical peptide previously studied in our laboratory (*67*) (*N*-acetyl-AEAAAKEAAAKEAAAKA-NH_2, uniformly labeled with ^{15}N and ^{13}C at A9 and A10).

Data Analysis. NMR spectra were processed using NMRPipe and NMRDraw (*68*) for 2D experiments and Varian Spinsight software for 1D experiments. The downfield ^{13}C line of adamantane [38.56 ppm relative to tetramethylsilane (TMS)] was used as an external reference for all ^{13}C spectra. Chemical shifts presented below are relative to TMS (^{13}C) or liquid ammonia (^{15}N). TALOS (*69*) was used for prediction of Vpu(1−40) ϕ and ψ torsion angles from ^{13}C and ^{15}N chemical shifts [after conversion of ^{13}C chemical shifts to a 2,2-dimethyl-2-silapentane-5-sulfonate (DSS) reference for TALOS calculations]. ^{15}N and ^{1}H relaxation times were obtained from the NMR data using the built-in curve-fitting functions in Spinsight. Cross-peak volumes were obtained from 2D $^{13}C-^{13}C$ NMR spectra using macros within NMRPipe.

Cross-peak volumes in 2D $^{15}N-^{13}C$ NMR spectra used to measure the extent of amide and side chain H−D exchange were obtained using custom peak fitting routines written in the Mathematica environment. For each sample in these experiments, the $^{15}N-^{13}C\alpha$ region of the 2D spectrum recorded prior to H−D exchange was fit to four to six Gaussian peaks. The number of Gaussian functions used was set equal to the number of apparent cross-peaks observed in each case. The observed ^{13}C and ^{15}N chemical shifts for each residue and the approximate NMR line widths were used as starting conditions for the iterative fitting routine. When the 2D $^{15}N-^{13}C$ NMR spectra recorded after exchange were fitted, all chemical shifts and line widths were fixed at the best-fit values for the unexchanged spectra, and only peak heights were allowed to vary. This method produced good fits to each of the experimental spectra, as judged by the small, random residuals. Good fits for side chain cross-peaks in $^{15}N-^{13}C$ spectra were obtained in a similar manner, using a single Gaussian peak in each case. Cross-peak volumes were normalized with respect to the total protein signal in each sample, based on signal intensities in 1D ^{13}C spectra.

RESULTS

Sample Characterization by SDS−PAGE and ^{31}P NMR. The amino acid sequence of the synthetic Vpu(1−40) peptides used in this study is shown in Figure 1A and includes the full N-terminal domain and a portion of the C-terminal cytoplasmic domain of full-length Vpu. The latter segment includes the conserved (*26*) $E^{28}YRK^{31}$ motif, proposed to play a role in ion channel stabilization and gating, along with a segment of the cytoplasmic domain of Vpu. The oligomeric state of Vpu(1−40) was examined by gel electrophoresis in SDS micelles, as shown in Figure 1B. A single band with an apparent molecular mass of 19−22 kDa is seen at both peptide concentrations shown. The arrow in Figure 1B indicates the expected location of monomeric Vpu(1−40) (monomer molecular mass of 4655 Da). On the basis of the observation that integral membrane peptides typically maintain helical structure in detergent micelles and exhibit faster than expected migration on PAGE gels (*70*, *71*), Vpu(1−40) seems to exist as a relatively stable oligomer of four to six peptide molecules in SDS micelles. There is some evidence for lower-molecular mass species, seen as a light smear below the stained protein band, perhaps indicating the existence of a monomer−oligomer equilibrium. Overall, this result is consistent with the pentameric structure estimated from single-channel conductance measurements (*39*), and is in contrast to earlier SDS−PAGE studies of a shorter Vpu peptide (Q2−E28 with an additional GRGGKKKK sequence at the C-terminus), for which only a stable monomer was observed under similar conditions (*34*).

Incorporation of 3 mol % Vpu(1−40) into mutilamellar 9:1 DOPC/DOPG liposomes did not affect the fluid bilayer structure of the membrane, as demonstrated in Figure 2. The static ^{31}P NMR powder patterns shown in panels B and D of Figure 2 have the characteristic 45 ppm chemical shift anisotropy (CSA) of fluid bilayers (*72*, *73*). There is, however, a distinct reduction in the sharp component of the powder pattern upon addition of peptide, which is consistent with the increased ^{31}P NMR line widths observed under MAS, as shown in panels A and C of Figure 2. The increased line widths may be due to increased lipid headgroup disorder

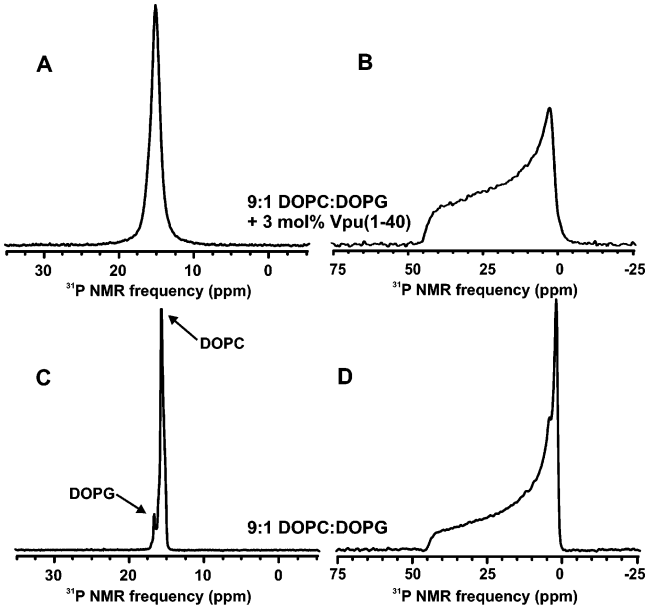

FIGURE 2: ^{31}P NMR spectra of 9:1 DOPC/DOPG bilayer membranes in the presence (A and B) or absence (C and D) of 3 mol % Vpu(1−40). Static spectra are shown in panels B and D, while spectra obtained at a MAS frequency of 10.00 kHz are shown in panels A and C. All spectra were obtained at 40 °C. Assignments for the ^{31}P resonances observed in the MAS spectra are shown in panel C.

in the presence of Vpu(1−40). A similar effect is seen for both the zwitterionic phosphatidylcholine and the anionic phosphatidylserine headgroups (resolved in the MAS spectra), indicating that nonpreferential peptide−lipid interactions are the cause of this effect. Additions of excess H_2O or up to 6 mol % Vpu(1−40) do not significantly alter the ^{31}P spectra that are obtained (not shown). This is consistent with the findings of Marassi and Crowell (*57*), who demonstrated that oriented bilayers of DOPC are relatively unperturbed even when equilibrated at 5% relative humidity, giving hydration levels lower than those reported here. Static ^{31}P NMR spectra of our Vpu(1−40) samples do not show significant isotropic components at any hydration level that was examined, ruling out the presence of rapidly tumbling small liposomes or micelles.

Static ^{31}P NMR spectra were not perturbed by exposure to MAS at frequencies up to 10 kHz for extended periods. MAS at 18 kHz was found to induce changes in the ^{31}P NMR spectrum attributable to disruption of the bilayer structure, possibly due to frictional heating of the sample at high MAS frequencies.

Hydration- and Position-Dependent Dynamics. ^{13}C MAS NMR spectra of 3 mol % Vpu(1−40)$_{AV}$ in multilamellar DOPC/DOPG vesicles are shown in panels B, D, and F of Figure 3, along with the spectra of membranes prepared in the absence of peptide (Figure 3A,C,E). The narrow resonances seen in both sets of spectra correspond to the natural abundance ^{13}C NMR signals of the lipids. As seen in Figure 3A−D, the lipid ^{13}C NMR chemical shifts do not change upon addition of Vpu(1−40), supporting the ^{31}P NMR observations as discussed above. In addition, spectra are shown for samples hydrated to 50% H_2O by weight (through addition of bulk water, Figure 3A,B) and for samples hydrated to 17% H_2O by weight (dry film in a hydration chamber, Figure 3C,D). There is no significant effect of

Table 1: ^{1}H, ^{13}C, and ^{15}N Relaxation Rates Measured for Vpu(1−40)$_{4A+6V}$ in DOPC/DOPG (9:1) Bilayer Membranes Containing 50 or 17% Water by Weight at Temperatures above and below the Lipid Phase Transition

relaxation rate	40 °C, 50% water	40 °C, 17% water	−50 °C
^{15}N T_2	ND	5.1 ms	18.9 ms
^{15}N T_1	ND	28.1 s	168.5 s
^{13}C T_2	1.4 ms (CO)	2.9 ms (CO)	4.2 ms (CO)
	3.3 ms (Ala Cβ)	2.2 ms (Ala Cα)	3.5 ms (Ala Cα)
	3.2 ms (Val Cγ)	3.9 ms (Ala Cβ)	7.5 ms (Ala Cβ)
		3.8 ms (Val Cγ)	4.7 ms (Val Cγ)
^{13}C T_1	ND	1.5 s (CO)	1.0 s (CO)
		1.2 s (Ala Cα)	0.9 s (Ala Cα)
		0.9 s (Ala Cβ)	0.4 s (Ala Cβ)
		1.0 s (Val Cγ)	0.4 s (Val Cγ)
^{13}C $T_{1\rho}$	3.8 ms (CO)	6.0 ms (CO)	18.4 ms (CO)
	4.1 ms (Ala Cβ)	3.4 ms (Ala Cα)	5.4 ms (Ala Cα)
	4.9 ms (Val Cγ)	5.2 ms (Ala Cβ)	7.5 ms (Ala Cβ)
		5.6 ms (Val Cγ)	7.7 ms (Val Cγ)
^{1}H(N) T_1	ND	484 ms	1.669 s
^{1}H $T_{1\rho}$	0.65 ms (CO)	2.0 ms (CO)	4.8 ms (CO)
	1.2 ms (Ala Cβ)	2.2 ms (Ala Cα)	4.6 ms (Ala Cα)
	1.4 ms (Val Cγ)	2.5 ms (Ala Cβ)	5.2 ms (Ala Cβ)
		2.4 ms (Val Cγ)	4.7 ms (Val Cγ)

hydration on the ^{13}C NMR spectra of DOPC/DOPG vesicles alone, with the relative intensities of lines obtained by DP (i.e., direct excitation of ^{13}C NMR signals with a single pulse) and CP (i.e., polarization transfer from ^{1}H spins) remaining unchanged. In contrast, the intensities of peaks arising from ^{13}C-labeled sites in Vpu(1−40)$_{AV}$ are strongly dependent on hydration level. Resolved signals from the labeled A18 and V25 residues in Vpu(1−40)$_{AV}$ are indicated by arrows in panels D and F of Figure 3. At 40 °C, there is little observable signal from the peptide at 50% hydration (Figure 3B) in either DP or CP spectra. At 17% hydration, however, there is a significant CP enhancement in the magnitude of the observed peptide signals (Figure 3D). This change must result from differences in the amplitudes and rates of peptide motion in bilayers at different hydration levels.

A reduction in the efficiency of ^{1}H−^{13}C CP for Vpu(1−40) in highly hydrated bilayers is likely due to an increase in motions occurring at frequencies near 10^5 s^{-1}. Such motions may lead to a reduction in the ^{1}H $T_{1\rho}$ of the peptide and a consequent reduction in CP transfer efficiency, as described for several integral membrane proteins (*74*−*76*). As indicated in Table 1, the ^{1}H and ^{13}C $T_{1\rho}$ relaxation times for Vpu(1−40) are significantly reduced in samples prepared at 50% hydration relative to those prepared at 17% hydration, consistent with an increase in the amplitudes of slow motions at frequencies near 10^5 s^{-1}. Motions occurring at these frequencies may also interfere with proton decoupling, producing an apparent loss of ^{13}C NMR signals in both CP and DP spectra. It has been suggested by Fares et al. (*74*) that localized bilayer undulations may occur on relevant time scales. The frequency and amplitude of such motions seem likely to be correlated with hydration level.

The ^{13}C CP NMR signal from Vpu(1−40) is enhanced at low temperatures (e.g., −50 °C as in Figure 3E,F). This signal enhancement is apparently due to suppression of motions occurring on relevant time scales, as indicated by the increased ^{1}H and ^{13}C $T_{1\rho}$ relaxation times observed in Vpu(1−40) samples at −50 °C. The gel−fluid phase transition for DOPC/DOPG bilayers is at −20 °C (*59*). Thus,

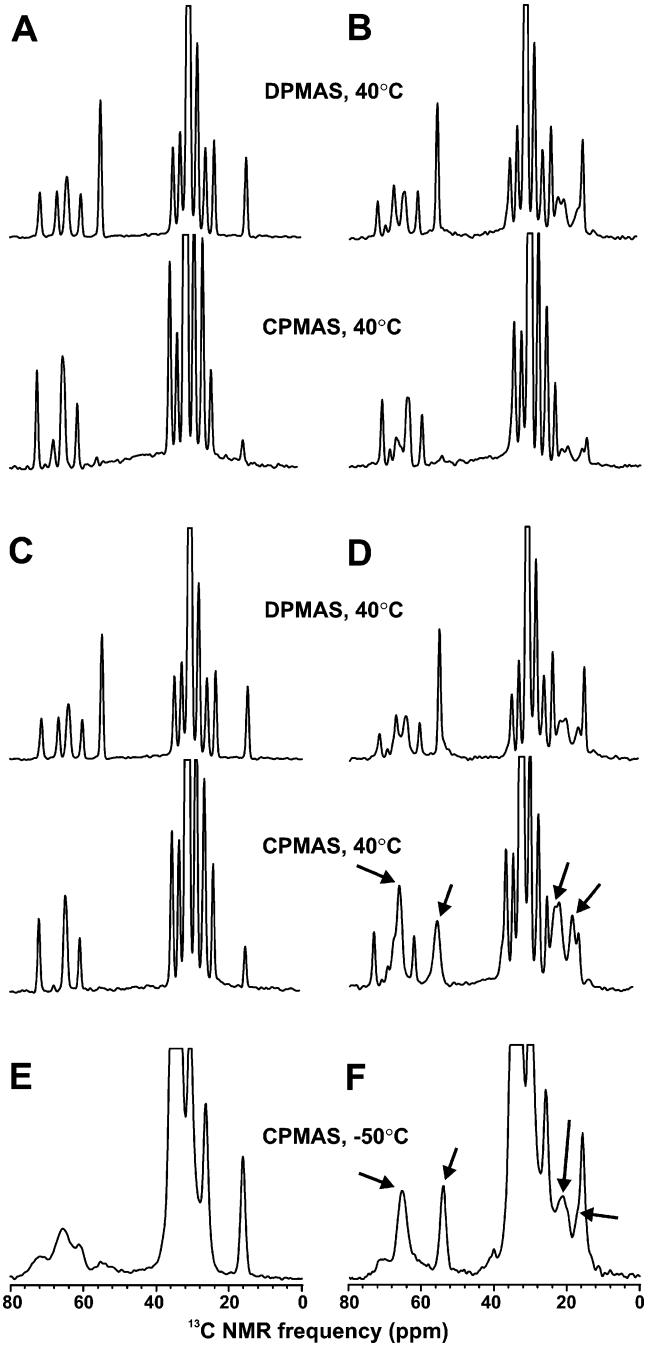

FIGURE 3: ^{13}C NMR spectra of DOPC/DOPG bilayer membranes with (B, D, and F) and without (A, C, and E) 3 mol % Vpu(1−40). Spectra obtained with direct polarization (DPMAS) and cross polariztion (CPMAS) are shown for samples containing 50% (A and B) or 17% (C−F) water by weight. Arrows in panels D and F indicate peaks arising from labeled sites in Vpu(1−40). Other peaks in each spectrum arise from natural-abundance ^{13}C of the phospholipids. All spectra were obtained at a MAS frequency of 9.00 kHz.

the signal enhancement may be due either to this phase transition or to overall freezing of the lipid/peptide/water mixture.

The effects of reduced $T_{1\rho}$ relaxation rates due to local bilayer fluctuations occurring at elevated hydration levels should also be evident in 2D ^{13}C−^{13}C NMR spectra. Panels A and D of Figure 4 show the 2D ^{13}C−^{13}C NMR spectrum of Vpu(1−40)$_{ASIYRL}$ at 40 °C and 50% (w/w) hydration, obtained with a 25 ms RAD mixing period. No cross-peak intensity can be discerned in this spectrum, providing further

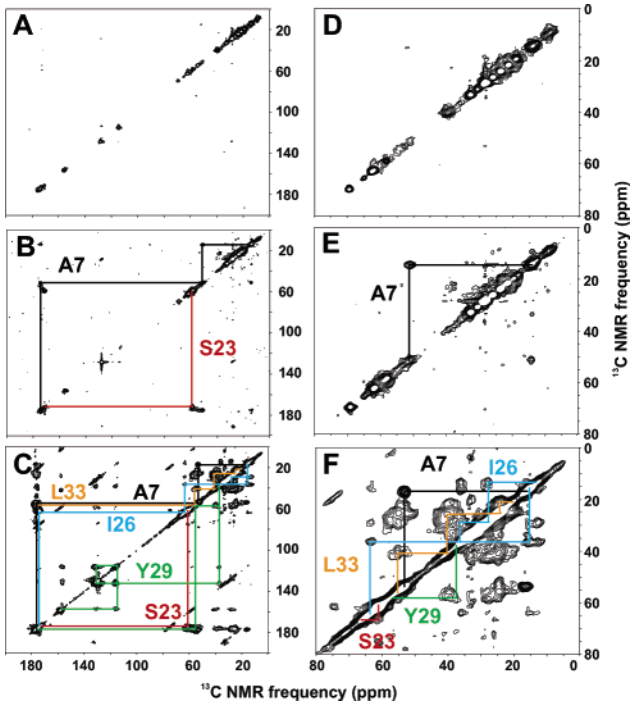

FIGURE 4: 2D ^{13}C−^{13}C NMR spectra of Vpu(1−40)$_{ASIYRL}$ at 3 mol % in 9:1 DOPC/DOPG bilayers. The full spectra are shown in panels A−C, while panels D−F show the aliphatic carbon regions. Results are shown for samples containing 50% H_2O (A and D) or 17% H_2O (B, C, E, and F) by weight. Sample temperatures are 40 (A, B, D, and E) or −50 °C (C and F). Resonance assignment pathways are indicated for all sites that can be assigned in each spectrum. All spectra were obtained at a MAS frequency of 9.00 kHz, with 25 (A, B, D, and E) or 10 ms (C and F) RAD mixing periods.

evidence for global motions occurring on a time scale that affects the NMR characteristics of the entire peptide sequence. Upon reduction of the total water content to 17% (w/w) (Figure 4B,E), intense CO−Cα cross-peaks are observed for A7 and S23. An intense A7 Cα−Cβ cross-peak is also seen in this spectrum. However, even with reduced bulk water content, most cross-peaks for Vpu(1−40)$_{ASIYRL}$ are absent, indicating local mobility within specific regions of Vpu(1−40), occurring on a time scale that interferes with ^{1}H−^{13}C CP and ^{13}C−^{13}C polarization transfer during the mixing period. In 2D spectra obtained at −50 °C with a 10 ms mixing period (Figure 4C,F), strong cross-peaks are observed for all labeled residues, consistent with elimination of most peptide motions. In addition, the total ^{13}C NMR signal per scan is higher, as described for 1D ^{13}C NMR spectra above. Figure 5 shows similar results for Vpu(1−40)$_{PVVAIR}$, where spectra obtained at 40 °C (Figure 5A,C) show cross-peaks for V12, V13, A14, and I24 only, while spectra obtained at −50 °C (Figure 5B,D) show cross-peaks for all labeled sites.

The ratios of Cα−Cβ cross-peak volumes observed at 40 and −50 °C for each residue with resolved cross-peaks in our labeled Vpu(1−40) samples are plotted in Figure 6. For this plot, cross-peak volumes are normalized to the total diagonal signal for peptide NMR lines. Cross-peak signals from P3, I26, Y29, R30, L33, R34, and K37 are most strongly suppressed at the higher temperature, suggesting that these specific residues are highly mobile and may lie outside the ordered helical portion of the TM domain. In addition, there is an attenuation of cross-peaks from all other residues

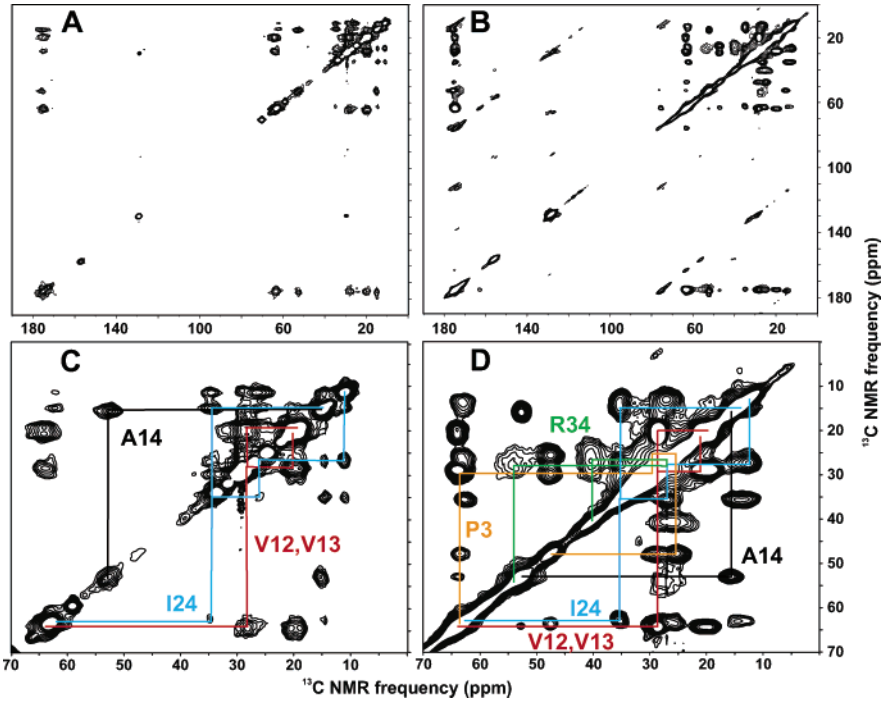

FIGURE 5: 2D ^{13}C−^{13}C NMR spectra of Vpu(1−40)$_{PVVAIR}$ at 3 mol % in 9:1 DOPC/DOPG bilayers. Spectra were obtained at 40 (A and C) or −50 °C (B and D). Full spectra are shown in panels A and B, while panels C and D show the aliphatic carbon regions. Resonance assignments possible at each temperature are shown in panels C and D. Samples contained 17% H_2O by weight. All spectra were obtained at a MAS frequency of 9.00 kHz, with 25 (A and C) or 10 ms (B and D) RAD mixing periods.

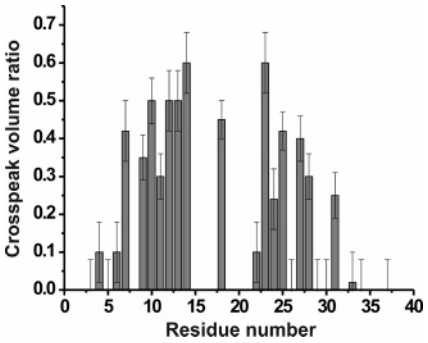

FIGURE 6: Ratios of Cα−Cβ cross-peak volumes in 2D ^{13}C−^{13}C NMR spectra of Vpu(1−40) samples at 40 °C to cross-peak volumes at −50 °C. Spectra were recorded as described in the legends of Figures 4 and 5. Cross-peak volumes were normalized to diagonal peak volumes before calculation of these ratios, to correct for variations in sample quantities and measurement conditions. Error bars indicate uncertainties calculated from the root-mean-square noise in the 2D ^{13}C−^{13}C NMR spectra.

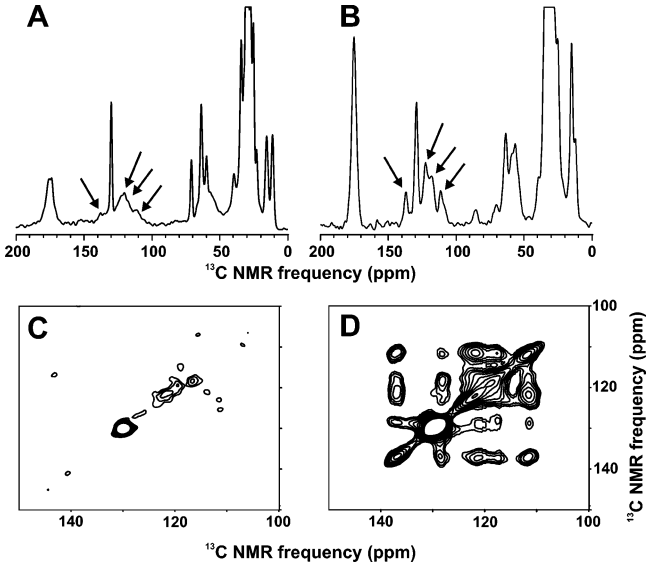

FIGURE 7: ^{13}C NMR spectra of Vpu(1−40)$_{IQIWK}$ at 3 mol % in 9:1 DOPC/DOPG bilayers. 1D (A and B) and 2D (C and D) ^{13}C NMR spectra were obtained at 40 (A and C) or −50 °C (B and D). Resolved resonances from W22 are indicated in each 1D ^{13}C spectrum. 2D NMR spectra show an expansion of the aromatic region of each spectrum. Samples contained 17% H_2O by weight and were obtained at a MAS frequency of 9.00 (A and C) or 8.00 kHz (B and D). 2D ^{13}C−^{13}C NMR spectra were obtained with 25 (C) or 10 ms (D) RAD mixing periods.

by 25−60% (despite the longer mixing periods in the 40 °C measurements), attributable to global motions of the peptide in the fluid phase bilayers (see below).

Despite being well within the TM domain of Vpu, very little intensity is observed for W22 side chain atoms in 1D or 2D ^{13}C NMR spectra of Vpu(1−40)$_{IQIWK}$ recorded at 40 °C (Figure 7). While the indole ring is unlikely to undergo rapid rotation around the χ_1 or χ_2 torsion angles, it is probable that large-amplitude, low-frequency motions occur which contribute to unfavorable relaxation behavior of the W22 side chain at 40 °C (*77*). As shown in Figure 7, this results in a significant reduction of the ^{13}C NMR signals and cross-peak intensities, as well as a broadening of the ^{13}C NMR lines for sites within the W22 side chain. This is in contrast to other residues within the TM domain of Vpu(1−40), which retain ^{13}C−^{13}C cross-peak intensity at 40 °C.

Measurements of ^{1}H, ^{15}N, and ^{13}C spin relaxation times on Vpu(1−40)$_{4A+6V}$ [a sample containing a 1:1 mixture of Vpu(1−40)$_{4A}$ and Vpu(1−40)$_{6V}$ in DOPC/DOPG bilayers] are summarized in Table 1. All relaxation times increase at the lower temperature with the exception of the ^{13}C T_1 values (attributable to more efficient spin−lattice relaxation by methyl rotation at the lower temperature). This is generally consistent with a reduced level of molecular motion at the

Table 2: ^{13}C and ^{15}N NMR Chemical Shifts (parts per million) for Vpu(1−40) at 3 mol % in DOPC/DOPG (9:1) Bilayer Membranes[a]

residue	CO	Cα	Cβ	Cγ	Cδ	Cε	Cζ,Nζ	N	φ (deg)	ψ (deg)
P3	175.3	63.4	29.5	20.0	47.4			137.4		
I4	175.3	63.4	35.5	27.9/15.5	12.3			117.3	−67	−37
Q5	175.7	56.9	26.2	35.0				118.5	−61	−41
I6	175.3	63.4	35.5	27.9/15.5	12.3			117.3	−70	−41
A7	176.0	52.4	15.3					119.5	−66	−31
I8[b]	174.8	63.0	35.0	27.0/14.0	15.9				−64	−40
V9	175.3	64.0	28.1	20.6/19.4				119.5	−63	−42
A10	176.0	52.2	15.2					119.5	−63	−34
L11	175.5	54.4	38.4	24.3	ND/20.4			117.6	−71	−26
V12	175.2	64.0	28.4	20.3/19.4				118.6	−62	−41
V13	175.2	64.0	28.4	20.3/19.4				118.6	−64	−39
A14	176.2	52.9	15.6					120.5	−63	−43
I15[b]	174.8	63.0	35.0	27.0/14.0	15.9				−66	−42
I16[b]	174.8	63.0	35.0	27.0/14.0	15.9				−65	−41
I17[b]	174.8	63.0	35.0	27.0/14.0	15.9				−63	−42
A18	176.6	54.5, *53.7*	15.2, *13.5*						−60	−41
I19[b]	174.8	63.0	35.0	27.0/14.0	15.9				−66	−41
V20[c]	175.2	64.3	28.5	(20.5/19.5)					−66	−43
V21[c]	175.2	64.3	28.5	(20.5/19.5)					−64	−42
W22	176.0	59.8	25.3	111.8 (C2), 121−124 (C4−C6), 117.9 (C7), 137.2 (C8), 128.6 (C9)		(126) (N1)		118.9	−63	−44
S23	173.4	60.3	60.4					114.8	−60	−35
I24	176.1	62.5	35.2	27.4/13.8				(121)	−68	−46
V25	175.1	65.7	28.0	21.5/20.0					−63	−42
I26	175.4	62.7	34.8	26.7/15.3	12.3			118.6	−65	−35
I27	ND	62.1	35.1	27.1/13.5	11.3			(120)	−67	−39
E28	ND	56.3	28.7	ND	ND			ND	−70	−34
Y29	ND	57.4	36.2	130.2	131.1	115.0	155.6	118.6	−98	6
R30	ND	56.0	27.8	24.8	41.4	83.5 (Nε)	156.5, 72.1	ND	−150	155
K31	ND	(55.3)	(34)	ND	26.4	38.8	32.4 (Nζ)	ND		
L33	(176.0)	53.4	39.2	23.8	ND			119.5		
R34	ND	(53.5)	(28)	(24)	(41.5)	84.5 (Nε)	(156.2), 72.4	(118)		
K37	ND	(56)	(31)	(24.3)	28.1	39.8	32.5 (Nζ)			

[a] Data were obtained from 2D $^{13}C-^{13}C$ and $^{13}C-^{15}N$ NMR spectra obtained at −50 °C. Shifts are referenced to TMS (^{13}C) or $NH_4(l)$ (^{15}N), and have a precision of ±0.2 ppm. Values in parentheses have a precision of ±0.5 ppm or worse, while values in italics indicate the chemical shift of minor species as discussed in the text. φ and ψ backbone torsion angles predicted using TALOS (*69*) are also given. [b] From a sample labeled at I8, I15, I16, I17, I19, I24, I26, and I27. [c] From a sample labeled at V9, V12, V13, V20, V21, and V25.

lower temperature. The shortest ^{13}C T_2 values measured for a sample with 17% hydration at 40 and −50 °C (2.1 and 3.8 ms, respectively) correspond to homogeneous ^{13}C NMR line widths of 151 and 84 Hz, respectively. At 40 °C, ^{13}C MAS NMR line widths are determined in part by T_2 relaxation. In samples with 50% hydration, further reductions in the ^{13}C T_2 values contribute to low signal intensities in 1D and 2D ^{13}C NMR spectra, along with inefficient CP due to short ^1H $T_{1\rho}$ relaxation times, especially for Cα and Cβ sites. At −50 °C, ^{13}C MAS NMR line widths are dominated by inhomogeneous broadening due to static structural disorder (see below).

Effects of sample hydration on dynamics, and hence on solid-state NMR signal intensities, depend on only the final hydration level, not on the method of hydration. For instance, addition of water to the sample used to obtain the spectrum in Figure 3D results in a sample with ^{13}C NMR characteristics similar to those shown in Figure 3B. This is also true for 2D $^{13}C-^{13}C$ NMR experiments performed as described in the legend of Figure 4. Optimized hydration levels are likely to be an important consideration for the preparation of membrane protein samples for solid-state NMR, as suggested previously by Marassi and Crowell (*57*). Minimally hydrated samples are also advantageous in MAS NMR due to the increased sample quantities within the rotor (and the concomitant increase in signal-to-noise ratios).

Vpu(1−40) Secondary Structure from NMR Chemical Shift Data. Chemical shift assignments for Vpu(1−40) are listed in Table 2. A nearly complete assignment of ^{13}C NMR chemical shifts was possible for labeled sites in Vpu(1−40) using 2D $^{13}C-^{13}C$ NMR spectra obtained at −50 °C as shown in Figures 4 and 5. ^{13}C NMR chemical shift assignments were determined from the expected pattern of cross-peaks for a given amino acid in combination with the literature values for the random coil chemical shifts (*78*). Sufficient spectral resolution was afforded by the deliberate choice of labeled residues in each sample such that spectral overlap in the Cα−Cβ region was minimized. Chemical shift assignments were not obtained for a number of carbonyl atoms due to insufficient resolution in this region of the 2D spectra. Likewise, several intra-side chain cross-peaks occur too close to the diagonal to be resolved. Selected ^{15}N assignments were made from 2D $^{15}N-^{13}C$ NMR spectra, such as those used for the H−D exchange experiments described in detail below.

Assignments for several residues were obtained from the $Vpu(1-40)_{6V}$ and $Vpu(1-40)_{4A}$ samples. Although these samples contain multiple labeled valine or alanine residues with unresolved NMR signals, the assignments are accurate to within roughly ±0.2 ppm. The ^{13}C line widths observed for each site in these samples range from 2 to 2.5 ppm, nearly identical to those seen for single valine or isoleucine labels, indicating that the chemical shifts for each residue type are nearly identical within the Vpu(1−40) transmembrane domain.

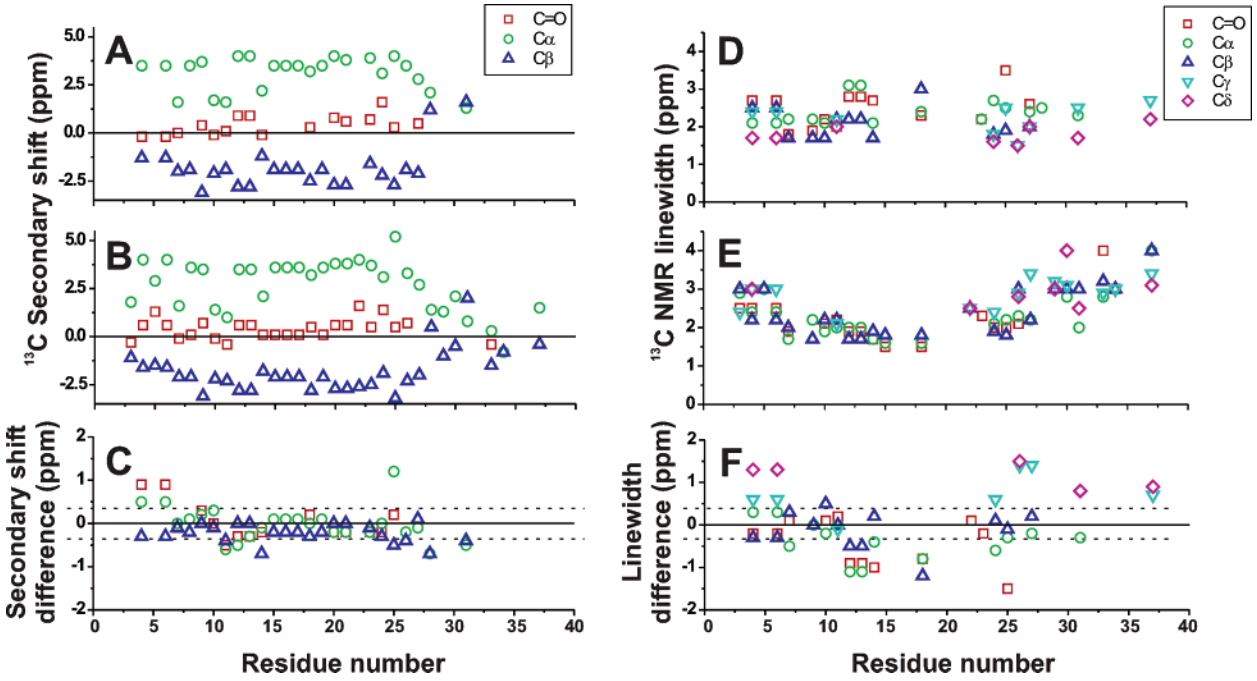

FIGURE 8: ^{13}C NMR chemical shifts and line widths for Vpu(1−40) at 3 mol % in DOPC/DOPG bilayers. The ^{13}C secondary shifts, calculated as the difference between observed chemical shifts and random coil shifts for a given amino acid (refs), are plotted for measurements made at 40 (A) and −50 °C (B). Similarly, the ^{13}C line widths (full width at half-maximum) measured at 40 (D) and −50 °C (E) are shown. Changes in chemical shifts (C) and line widths (F) with a reduction in temperature from 40 to −50 °C are also shown. Dashed lines in panels C and F indicate the estimated uncertainties in chemical shift and line width difference measurements, respectively.

Deviations of the CO, Cα, and Cβ chemical shifts in Vpu(1−40) from random coil values (*79*, *80*) (i.e., secondary shifts) are plotted in panels A and B of Figure 8, along with the changes in chemical shifts in gel phase versus fluid phase bilayers (Figure 8C). A negative secondary shift for Cβ and positive shifts for CO and Cα indicate α-helical secondary structure, particularly when several consecutive residues exhibit the same pattern of secondary shifts. Helical secondary shifts are observed for residues 7−27 at 40 °C and residues 3−27 at −50 °C. Residues 28−34 and 37 exhibit secondary shifts that are apparently inconsistent with regular secondary structures. For all sites that are visible in NMR spectra at both temperatures, the chemical shifts are independent of temperature, implying the absence of significant structural changes with temperature and bilayer phase.

Predictions of backbone ϕ and ψ torsion angles for residues 4−30 of Vpu(1−40) at −50 °C were obtained with TALOS (*69*), which compares the experimentally determined ^{15}N and ^{13}C NMR chemical shifts with shifts in a database of proteins with known high-resolution structures and known chemical shift assignments. The predicted torsion angles are given in Table 2, and are consistent with an α-helix extending from I4 (or earlier) to E28. Due to gaps in the chemical shift data, no TALOS predictions are available for residues 1−3 and 31−40.

^{13}C NMR line widths for Vpu(1−40) are plotted in Figure 8D−F. At −50 °C, all labeled sites in residues 7−25 exhibit line widths of 1.5−2.5 ppm, as observed for other structurally ordered protein and peptide systems in rigid, noncrystalline environments (*81*, *82*). Significantly larger line widths are observed at residues 3−6, 26−34, and 37, indicating greater disorder. Together with the data in Figure 6 and Table 2, the line width data indicate a highly ordered α-helical segment from A7 through V25. I26 and I27 are also part of the α-helix, but are apparently less well ordered. Residues 28−37 are outside the α-helix and are generally more disordered at −50 °C and exhibit greater dynamics at 40 °C. Note that line width data are unavailable for residues whose chemical shift assignments were made from samples containing the Vpu(1−40)$_{6V}$ and Vpu(1−40)$_{8I}$ peptides.

As shown in Figure 8F, several residues in the ordered α-helical segment exhibit narrower ^{13}C NMR lines at −50 °C than at 40 °C. This may be due in part to an overall increase in conformational order in the gel phase of the DOPC/DOPG bilayers and in part to the longer ^{13}C T_2 relaxation times at the lower temperature (see above). Conversely, Cγ NMR lines of I4, I6, I26, and I27 are significantly broader at −50 °C than at 40 °C, most likely due to motional narrowing (at the higher temperature) of the inhomogeneously broadened low-temperature lines. Line narrowing at the higher temperature is also observed in the ^{15}N MAS NMR spectra of Vpu(1−40)$_{PVVAIR}$ and Vpu(1−40)$_{VALIEK}$ shown in panels A and B of Figure 9, respectively, particularly for the ^{15}N NMR lines of the mobile R34 and K31 side chains (at 60−80 and 30 ppm, respectively). A similar motion-induced averaging of inhomogeneous broadening has been observed for viral fusion peptides in fluid bilayer environments (*75*). No ^{15}N NMR line is observed for the K37 side chain at 40 °C, likely due to dynamic disorder near the C-terminus of Vpu(1−40).

Rigid-Body Dynamics and TM Helix Tilt. The overall reduction in ^{13}C MAS NMR signals for residues 7−25 at 40 °C apparent in Figures 3−7 (compared with signals for these residues at −50 °C) is attributable to the rigid-body dynamics of Vpu(1−40) in fluid lipid bilayers. Proteins embedded in lipid bilayers are known to undergo a number of rigid-body motions, including rapid axial rotation and lower-frequency "wobble" motions around multiple axes (*74*,

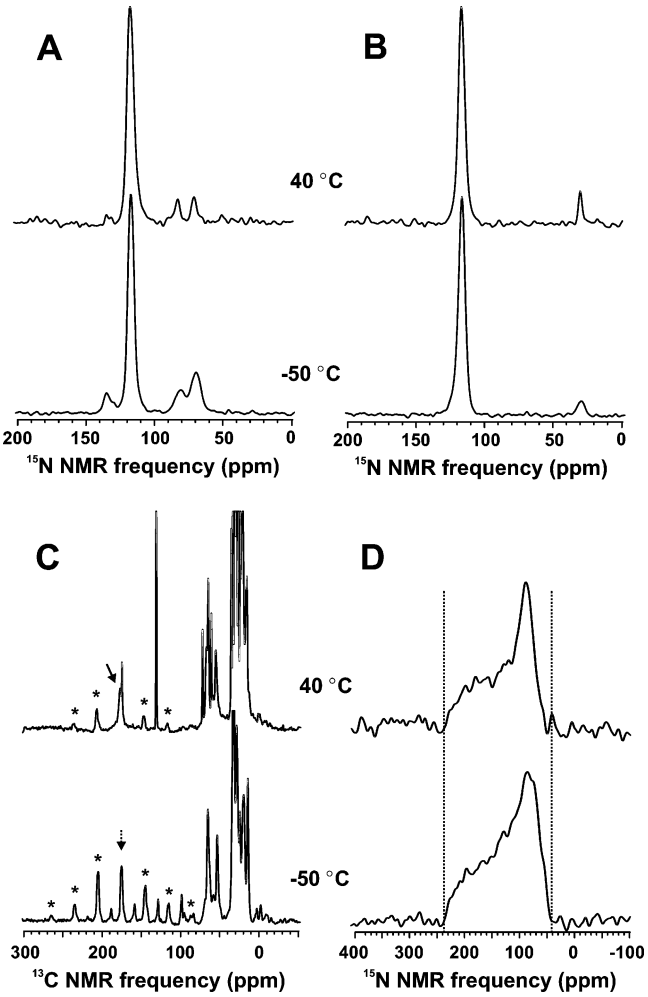

FIGURE 9: Effect of temperature on backbone carbonyl ^{13}C and amide ^{15}N chemical shift anisotropies in Vpu(1−40). (A) ^{15}N MAS NMR spectra of Vpu(1−40)$_{PVVAIR}$. (B) ^{15}N MAS NMR spectra of Vpu(1−40)$_{ASIYRL}$. (C) ^{13}C NMR spectra of a sample containing equal amounts of Vpu(1−40)$_{4A}$ and Vpu(1−40)$_{6V}$, obtained at a MAS frequency of 3.00 kHz at the indicated temperatures. (D) Static ^{15}N NMR spectra of the same sample.

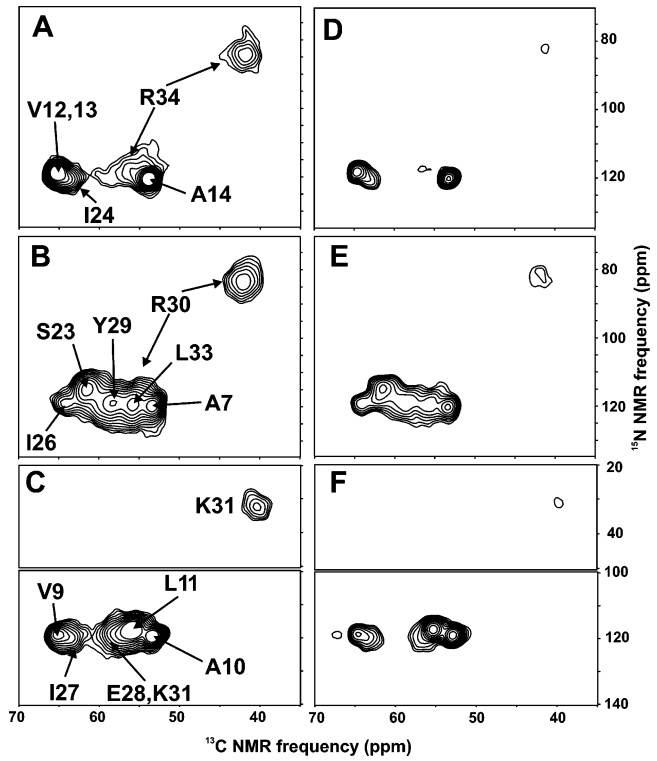

FIGURE 10: H−D exchange in Vpu(1−40) monitored by 2D ^{15}N−^{13}C NMR spectroscopy. Spectra of Vpu(1−40) at 3 mol % in DOPC/DOPG bilayers are shown for samples in H_2O (A−C) and after exchange with D_2O for 2 h (D−F). Cross-peak assignments are indicated for spectra of Vpu(1−40)$_{PVVAIR}$ (A and D), Vpu(1−40)$_{ASIYRL}$ (B and E), and Vpu(1−40)$_{VALIEK}$ (C and F). All spectra were acquired at −50 °C, at a MAS frequency of 9.00 kHz. Contour levels in unexchanged (A−C) and exchanged (D−F) spectra have been adjusted for variations in sample quantities based on signal intensities in 1D ^{13}C NMR spectra, and are therefore directly comparable.

83−*86*). These motions, which affect the ordered α-helical segment of Vpu(1−40), are distinct from the site-specific variations in local mobility discussed above, which differentiate ordered from dynamically disordered segments.

Figure 9C shows 1D ^{13}C MAS spectra of Vpu(1−40)$_{4A+6V}$, in which only residues within the most highly ordered portion of the TM domain have been labeled. ^{13}CO NMR signals for this sample are primarily sensitive to rigid-body motions. At a MAS frequency of 3.0 kHz, the ^{13}CO NMR line is split into a series of spinning sidebands whose intensities are determined by the motionally averaged CSA tensors of the backbone carbonyl sites. The spectrum recorded at 40 °C clearly shows less intense sidebands than the spectrum at −50 °C. This is attributable to averaging of the ^{13}CO CSA by axial rotational diffusion on a time scale of approximately ≤10 μs. CSA principal values obtained from fitting the experimental ^{13}CO MAS sideband intensities (*87*) are as follows: $\delta_{11} = 250$ ppm, $\delta_{22} = 182$ ppm, and $\delta_{33} = 96$ ppm at −50 °C and $\delta_{11} = 215$ ppm, $\delta_{22} = 194$ ppm, and $\delta_{33} = 119$ ppm at 40 °C. The low-temperature values are typical of carbonyl sites in a rigid peptide backbone. The high-temperature values represent a fit to the total sideband intensities for multiple sites with inequivalent motionally averaged CSA tensors. Detailed interpretation of the ^{13}CO MAS sideband intensities at 40 °C will require full quantum mechanical simulations of the dipole-coupled ^{13}C spin systems in the labeled residues. However, the observed reduction in sideband intensities is qualitatively consistent with rapid rotation of an α-helix about an axis perpendicular to the bilayer plane, with a small helical tilt, as suggested by previous FTIR and NMR studies of Vpu TM domain peptides (*29*, *34*, *45*).

Static ^{15}N CSA powder pattern spectra shown in Figure 9D are much less sensitive to temperature. The ^{15}N powder pattern width is reduced by a factor of less than 0.86 at 40 °C, corresponding to a helical tilt angle of ≤20°, given that the backbone amide ^{15}N CSA tensor is approximately axially symmetric with the unique axis approximately parallel to the long axis of the α-helix (*88*).

H−*D Exchange of Vpu(1*−*40) in DOPC/DOPG Bilayer Membranes.* Figure 10 shows 2D ^{15}N−^{13}C NMR spectra of Vpu(1−40) in DOPC/DOPG bilayers before (Figure 10A−C) and after (Figure 10D−F) H−D exchange for 2 h in D_2O at pH 6−7 and room temperature. Assignments of the amide ^{15}N−^{13}Cα cross-peaks are based on the assigned ^{13}Cα NMR chemical shifts. Following exchange, there is a site-specific decrease in the cross-peak volumes. Since the nuclear spin magnetization in these measurements originates primarily from the amide protons, changes in cross-peak volumes

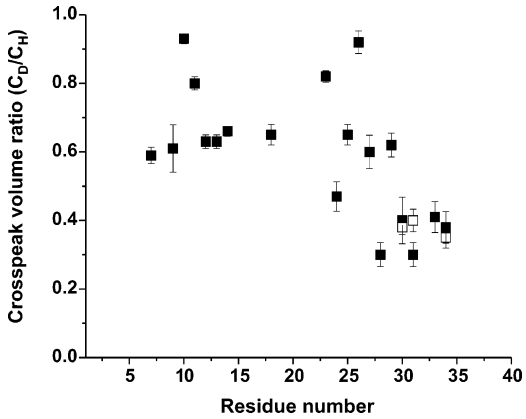

FIGURE 11: Summary of H−D exchange data for Vpu(1−40) in DOPC/DOPG membranes. The degree of exchange at each site is plotted as the fraction of cross-peak volume remaining in 2D $^{15}N-^{13}C$ NMR spectra (as in Figure 9) after exchange in D_2O for 2 h. Results for backbone N−Cα cross-peaks (■) and for side chain N−C cross-peaks (□) are plotted for each labeled amino acid. Error bars indicate 95% confidence intervals derived from least-squares fits of cross-peaks to Gaussian line shapes.

reflect the extent of amide H−D exchange in a site-specific manner.

Figure 11 shows the ratios of $^{15}N-^{13}C\alpha$ cross-peak volumes after H−D exchange to cross-peak volumes before exchange. Data for ^{15}N-containing side chains (R30, K31, and R34) are also plotted in Figure 11. Residues 28 and 30−34 exhibit greater than 60% H−D exchange, while the remaining residues are exchanged to a significantly lower extent. Rapid exchange of amide protons for the C-terminal residues is indicative of both exposure to the aqueous environment and increased backbone accessibility. The latter is likely related to the increased mobility and conformational disorder at these sites implied by the ^{13}C NMR line width and $^{13}C-^{13}C$ cross-peak intensity data presented above. Residual $^{15}N-^{13}C$ cross-peak intensity for rapidly exchanging sites after H−D exchange is attributable in part to $^{1}H-^{15}N$ CP from nonexchangeable protons (e.g., Hα and Hβ, accounting for 10−15% of the $^{15}N-^{13}C\alpha$ cross-peak intensity in control measurements on the soluble, helical peptide *N*-acetyl-AEAAAKEAAAKEAAAKA-NH_2) and in part to incomplete dispersion of D_2O within MLVs. Note that the extent of exchange for side chain sites is approximately the same as the maximum extent of exchange for backbone sites. This implies that the maximum possible exchange at 2 h for the Vpu(1−40) residues investigated here is ∼65−70%.

It is tempting to correlate the variations seen in the extent of H−D exchange for the more slowly exchanging sites with the anticipated ion channel structure of Vpu(1−40), in which residues lining the solvent-exposed pore may exchange more rapidly than those at protein−protein or protein−lipid interfaces, as seen for the M2 channel (*55*). Consistent with the results presented here, Kukol and Arkin (*29*) observe exchange of at least 15−35% of the amide protons in the TM domain of Vpu(1−31) in DMPC bilayers, as monitored by FTIR spectroscopy. It has been suggested that such exchange within a transmembrane domain requires the presence of water within the bilayer, and may imply the presence of an aqueous pore (*55*). However, the intrinsic sequence-dependent variability of amide protein H−D exchange rates (*89*) may create 10-fold variations in exchange rates for unfolded peptides, preventing a detailed

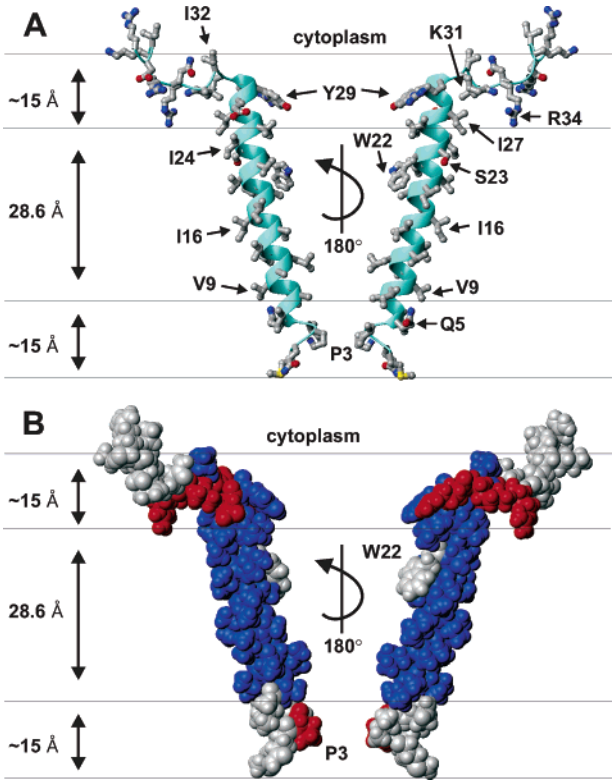

FIGURE 12: Structural model for the Vpu(1−40) monomer based on the solid-state MAS NMR data. Ball-and-stick (A) and space-filling models (B) of Vpu(1−40) are shown, with residues colored by the degree of structural order in panel B. Blue sites are well-ordered, exhibiting narrow ^{13}C line widths and low mobility, while red residues exhibit significant disorder and increased mobility. Residues for which no data are available are gray. Several amino acid side chains are labeled to provide a visual reference for the orientation of Vpu(1−40), and a 180° rotation is applied between the two structures. The overall topology of Vpu(1−40) as shown is consistent with data presented in this paper. Backbone torsion angles were set to the values predicted by TALOS from the ^{13}C chemical shift data, and side chain conformations were set using SCWRL 3.0 (*100*). The backbone structure of residues 31−40 was set arbitrarily. The hydrophobic core thickness of the depicted bilayer is 28.6 Å, while the headgroup is ∼15 Å on each side, consistent with the known structure of DOPC membranes (*101*). Models were prepared in MOLMOL (*102*).

analysis of the exchange data presented here. A more detailed measurement of the site-specific H−D exchange rates may provide insight into the channel organization of Vpu, as suggested by studies of H−D exchange in integral membrane proteins using NMR studies of oriented bilayers (*55*) or FTIR spectroscopy (*90*).

DISCUSSION

A Structural Model for Vpu(1−40) and Its Implications. The structural data obtained in this work are summarized in the model shown in Figure 12, representing a single Vpu-(1−40) peptide within a putative oligomer. On the basis of the observation of α-helical ^{13}C NMR chemical shifts for all labeled residues in the segment of residues 3−27, the observation of nonhelical chemical shifts for residues 28, 31, 33, 34, and 37 (Figure 8A,B), and the TALOS predictions of ϕ and ψ backbone torsion angles (Table 2), the helical segment of the TM domain includes residues 3−27 and may extend to the N-terminus. The observation of relatively broad ^{13}C NMR lines for residues 3−6, 26, 27, 29−31, 33, 34,

and 37 at −50 °C (Figure 8E) suggests structural heterogeneity at these sites, including partial fraying of the C-terminal end of the helical segment (residues 26 and 27). The extreme N-terminal and C-terminal portions of Vpu(1−40), including residues 3−6, 26, 29, 30, 33, 34, and 37, appear to exhibit increased mobility at 40 °C, based on the strong attenuation of their ^{13}C NMR signals (Figure 6).

The 13° tilt of the TM helix relative to the bilayer normal depicted in Figure 12 and the orientation about the helix axis are chosen to follow pore models in which W22 is facing the bilayer outside the channel (*34*). Park et al. report a 13° tilt for Vpu(2−30), based on solid-state NMR of oriented DOPC/DOPG bilayer membranes (*34*), while Kukol and Arkin report a 6.5° tilt, based on FTIR measurements of Vpu in DMPC bilayers (*29*). Similarly, their values for rotation differ significantly, as reflected by the left-handed versus right-handed packing of adjacent helices in the bundle models developed by each group, and the inside versus outside orientation of W22 in the two models. A small helical tilt angle (<20°) is suggested by the slight reduction in ^{15}N CSA powder pattern width at 40 °C shown in Figure 9D, consistent with these earlier estimates of helix tilt.

The mobility of Vpu(1−40) on SDS−PAGE gels (Figure 1B) suggests that a stable oligomer containing four to six peptide molecules is formed in SDS micelles. This is consistent with the molecular modeling studies performed by several groups (*38*−*42*). Chemically tethered tetramers and pentamers of the Vpu TM domain have been shown to form ion channels with a conductance similar to that of the native protein (*91*). The NMR data presented here may reflect the structure of Vpu(1−40) within an oligomeric channel, although we do not have direct evidence of ion channel activity in our samples. We observe a single, narrow peak for each site within the ordered TM domain of Vpu(1−40) (except for A18; see below), with ^{13}C MAS NMR line widths essentially the same as those observed in structurally ordered peptide−antibody complex (*82*) and amyloid fibril (*81*, *92*) samples. Assuming the formation of oligomers with lifetimes greater than the NMR time scale (roughly 20 ms, dictated by the approximate 0.5 ppm lower limit on detectable ^{13}C NMR chemical shift differences), the ^{13}C MAS NMR line widths are consistent with a symmetric structure for the Vpu oligomer in DOPC/DOPG bilayers. The assumption of stable oligomer formation also implies that the rapid axial rotation of Vpu(1−40) indicated by the ^{13}C MAS sideband patterns in Figure 9C is actually rotational diffusion of the entire oligomer about an axis normal to the membrane surface. This is similar to what has been observed for a number of small integral membrane proteins (*74*, *85*, *86*, *93*−*95*), and even for larger proteins, such as rhodopsin or bacteriorhodopsin reconstituted into artificial bilayers (*76*, *96*).

That we observe a single MAS NMR line for all resolved ^{13}C-labeled residues, other than A18, may argue against a proposed model for ion channel gating, in which the TM helices in the oligomer rotate by large angles relative to one another (*24*, *43*), placing W22 either within (closed state) or outside (open state) the channel. However, we do observe two distinct sets of ^{13}C chemical shifts for A18 (2:1 ratio). This residue lies directly beneath W22 in the model shown in Figure 12 such that its ^{13}C NMR frequencies may be subject to ring-current shifts from the side chain indole group of W22. The presence of two distinct W22 side chain conformers with populations in a 2:1 ratio might explain the splitting of A18 ^{13}C NMR lines. However, a single ^{13}C NMR line is observed for each site within W22 at −50 °C (see Figure 7), suggesting that the W22 side chain does not populate multiple distinct conformations. In addition, in vacuo molecular dynamics simulations at elevated temperatures indicate that the range of possible distances between Cβ of A18 and the center of the six-membered ring of the W22 indole group is roughly 3.5−7.0 Å when residues 13−28 are restrained to an α-helical structure. It appears unlikely that ring current shifts large enough to account for the observed A18 splittings (1.7 ppm for Cβ at −50 °C) could occur with this distance range (*97*). In addition, the side chain carbon sites of W22 show single, relatively sharp ^{13}C NMR lines (e.g., 2.5 ppm line width for Cβ of W22 at −50 °C), arguing against multiple side chain conformations.

An alternative explanation for the observed splitting of A18 ^{13}C NMR signals may be that this site resides at the helix−helix interface in Vpu(1−40) oligomers and that two distinct modes of helix−helix interaction are present (involving relatively small helix rotations, in contrast to the gating mechanism discussed in refs *24* and *43*). Sequence analysis of Vpu shows that A18 resides within a conserved alanine zipper motif (*98*) (here composed of A7, A10, A14, and A18) which forms a likely surface for helix−helix associations within the Vpu TM domain oligomer. The splitting of A18 NMR signals could also result from an oligomer−monomer equilibrium. Further experiments are necessary to distinguish between these possibilities.

As described above, the loss of signal intensity and the concurrent increase in aromatic ^{13}C NMR line widths for W22 at 40 °C reflect increased amplitudes of side chain motion. Side chain mobility is consistent with W22 exclusively oriented to face the lipid environment. Localization of this residue at either a helix−helix interface or within the lumen of an ion-conducting channel might inhibit side chain mobility. Thus, our data support a model for Vpu channel activity in which W22 does not play a direct role in gating. It is likely that this highly conserved residue instead plays a role in orienting the Vpu TM domain relative to the lipid−water interface, as suggested by studies of model hydrophobic peptides (*99*). The presence of a putative alanine zipper motif suggests a right-handed packing of helices, allowing favorable interhelical contacts along the length of the zipper (*98*). Taken together, our results are consistent with a right-handed bundle of Vpu(1−40) monomers with W22 outside the pore, and imply that gating of channel activity is unlikely to involve large-amplitude reorientations of the individual helices.

The apparent flexibility and disorder of the conserved EYRK motif, indicated by strong attenuation of ^{13}C NMR signals for Y29 and R30 at 40 °C (Figure 6) and the relatively broad ^{13}C NMR lines for this motif at −50 °C (Figure 7E), are inconsistent with recent models of the Vpu oligomer, in which these residues form a clamp around the outer surface of the TM helix bundle with intermolecular electrostatic and hydrogen bonding interactions between E28 and K31 of one helix and Y29 of a second helix (*39*, *44*). Our results instead favor models in which this region is destabilized relative to the transmembrane domain (*36*), although the E28−K31 salt bridge proposed by Srmala et al. (*36*) seems unlikely to form in the presence of charged lipid headgroups. It is plausible

that the EYRK motif simply provides a polar environment at the mouth of the Vpu channel, and that the motions of these residues may play a role in gating the ion conductance. In contrast with the large-amplitude motions experienced by K37, leading to nearly complete attenuation of its ^{13}C and ^{15}N NMR signals at 40 °C, the relatively high intensity of the ^{13}C and ^{15}N signals from K31 at 40 °C implies restricted-amplitude motions, consistent with limited conformational flexibility at this site.

Our data rule out formation of a second, amphipathic helix by residues 30−40 in Vpu(1−40), as indicated by solution NMR studies of Vpu(28−81) (*33*). Our data appear to be more consistent with earlier models of full-length Vpu, in which residues 30−35/36 are not part of the second helix, but instead form a flexible linker (*28*, *30*, *31*). However, the possibility clearly exists that truncation of the cytoplasmic domain of Vpu may inhibit helix formation by residues 30−40. Detailed structural studies of full-length Vpu in a membrane environment will undoubtedly be required to obtain an improved description of the cytoplasmic domain.

Methodological Significance. The measurements described above illustrate the complexity of applying solid-state MAS NMR methods to integral membrane proteins, particularly viroporins, and demonstrate a number of strategies that are likely to be of general utility. The quality of MAS NMR data on systems with multiple uniformly labeled residues, including the signal intensities and line widths in 1D and 2D ^{13}C NMR spectra, depends strongly on hydration level and temperature. At temperatures where the phospholipid bilayer is in the fluid phase, minimal hydration consistent with bilayer formation appears to give the best results. Higher hydration levels apparently lead to molecular motions that interfere with CP and possibly with proton decoupling. Lower temperatures, where the bilayer is in a gel phase and bulk water is frozen, produce stronger ^{13}C MAS NMR signals, narrower lines for certain sites, and detectable signals for sites that are invisible in the fluid phase. Comparison of signal intensities in low-temperature and high-temperature spectra allows the identification of highly dynamic and relatively rigid segments of an integral membrane protein. MAS NMR line widths at low temperatures can be used to identify structurally ordered and structurally disordered segments. Helical and nonhelical segments in integral membrane proteins can be identified from measurements of secondary shifts in ^{13}C MAS NMR spectra.

For proteins or protein fragments that are sufficiently small that they can be chemically synthesized, preparation of a series of samples with different sets of uniformly ^{15}N- and ^{13}C-labeled (six or more labeled residues in each sample) allows ^{13}C and ^{15}N NMR chemical shift assignments to be made from well-resolved 2D $^{13}C-^{13}C$ and $^{15}N-^{13}C$ NMR spectra. Site-specific line width and signal intensity measurements are then possible. While this approach is generally limited to proteins requiring synthesis and chemical ligation of no more than two 40-residue segments, it circumvents the difficult task of making unambiguous chemical shift assignments for uniformly labeled proteins with NMR line widths greater than 1 ppm.

Measurements of H−D exchange in a bilayer environment provide information about solvent exposure and local secondary structure stability. As shown by our experiments on Vpu(1−40), site-specific H−D exchange data can be acquired by detection of cross-peak intensities in 2D $^{15}N-^{13}C$ NMR spectra, for both backbone amide and side chain nitrogen sites. H−D exchange can be used to distinguish protein segments that lie within the bilayer from those outside. It may also prove to be possible to identify residues that line a TM pore or channel in this way, as shown previously for H−D exchange measurements detected by other means (*55*, *90*).

ACKNOWLEDGMENT

We thank Dr. Anant Paravastu for assistance with analysis of the H−D exchange spectra and acknowledge helpful discussions with Drs. Nathan Oyler, Robert Havlin, and Aneta Petkova.

REFERENCES

1. Cohen, E. A., Terwilliger, E. F., Sodroski, J. G., and Haseltine, W. A. (1988) Identification of a protein encoded by the Vpu gene of HIV-1, *Nature 334*, 532−534.
2. Strebel, K., Klimkait, T., and Martin, M. A. (1988) A novel gene of HIV-1, Vpu, and its 16-kilodalton product, *Science 241*, 1221−1223.
3. Schubert, U., Bour, S., FerrerMontiel, A. V., Montal, M., Maldarelli, F., and Strebel, K. (1996) The two biological activities of human immunodeficiency virus type 1 Vpu protein involve two separable structural domains, *J. Virol. 70*, 809−819.
4. Marassi, F. M., Ma, C., Gratkowski, H., Straus, S. K., Strebel, K., Oblatt-Montal, M., Montal, M., and Opella, S. J. (1999) Correlation of the structural and functional domains in the membrane protein Vpu from HIV-1, *Proc. Natl. Acad. Sci. U.S.A. 96*, 14336−14341.
5. Maldarelli, F., Chen, M. Y., Willey, R. L., and Strebel, K. (1993) Human-immunodeficiency-virus type-1 Vpu protein is an oligomeric type-I integral membrane-protein, *J. Virol. 67*, 5056−5061.
6. Ewart, G. D., Sutherland, T., Gage, P. W., and Cox, G. B. (1996) The Vpu protein of human immunodeficiency virus type 1 forms cation-selective ion channels, *J. Virol. 70*, 7108−7115.
7. Schubert, U., FerrerMontiel, A. V., OblattMontal, M., Henklein, P., Strebel, K., and Montal, M. (1996) Identification of an ion channel activity of the Vpu transmembrane domain and its involvement in the regulation of virus release from HIV-1-infected cells, *FEBS Lett. 398*, 12−18.
8. Terwilliger, E. F., Cohen, E. A., Lu, Y. C., Sodroski, J. G., and Haseltine, W. A. (1989) Functional role of human immunodeficiency virus type-1 Vpu, *Proc. Natl. Acad. Sci. U.S.A. 86*, 5163−5167.
9. Klimkait, T., Strebel, K., Hoggan, M. D., Martin, M. A., and Orenstein, J. M. (1990) The human immunodeficiency virus type 1-specific protein Vpu Is required for efficient virus maturation and release, *J. Virol. 64*, 621−629.
10. Schubert, U., Henklein, P., Bour, S., Ferrermontiel, A. V., Oblattmontal, M., Montal, M., and Strebel, K. (1995) Virus release from HIV-1-infected cells is regulated by an ion-channel activity of Vpu, *AIDS Res. Hum. Retroviruses 11*, S114.
11. Varthakavi, V., Smith, R. M., Bour, S. P., Strebel, K., and Spearman, P. (2003) Viral protein U counteracts a human host cell restriction that inhibits HIV-1 particle production, *Proc. Natl. Acad. Sci. U.S.A. 100*, 15154−15159.
12. Hsu, K., Seharaseyon, J., Dong, P. H., Bour, S., and Marban, E. (2004) Mutual functional destruction of HIV-1 Vpu and host TASK-1 channel, *Mol. Cell 14*, 259−267.
13. Hout, D. R., Gomez, M. L., Pacyniak, E., Gomez, L. M., Inbody, S. H., Mulcahy, E. R., Culley, N., Pinson, D. M., Powers, M. F., Wong, S. W., and Stephens, E. B. (2005) Scrambling of the amino acids within the transmembrane domain of Vpu results in a simian-human immunodeficiency virus ($SHIV_{TM}$) that is less pathogenic for pig-tailed macaques, *Virology* (in press).
14. Paul, M., Mazumder, S., Raja, N., and Jabbar, M. A. (1998) Mutational analysis of the human immunodeficiency virus type 1 Vpu transmembrane domain that promotes the enhanced release

of virus-like particles from the plasma membrane of mammalian cells, *J. Virol. 72*, 1270−1279.
15. Tiganos, E., Friborg, J., Allain, B., Daniel, N. G., Yao, X. J., and Cohen, E. A. (1998) Structural and functional analysis of the membrane-spanning domain of the human immunodeficiency virus type 1 Vpu protein, *Virology 251*, 96−107.
16. Willey, R. L., Maldarelli, F., Martin, M. A., and Strebel, K. (1992) Human-immunodeficiency-virus type-1 Vpu protein induces rapid degradation of CD4, *J. Virol. 66*, 7193−7200.
17. Willey, R. L., Maldarelli, F., Martin, M. A., and Strebel, K. (1992) Human-immunodeficiency-virus type-1 Vpu protein regulates the formation of intracellular gp160-CD4 complexes, *J. Virol. 66*, 226−234.
18. Chen, M. Y., Maldarelli, F., Karczewski, M. K., Willey, R. L., and Strebel, K. (1993) Human-immunodeficiency-virus type-1 Vpu protein induces degradation of CD4 *in vitro*: The cytoplasmic domain of CD4 contributes to Vpu sensitivity, *J. Virol. 67*, 3877−3884.
19. Bour, S., Schubert, U., and Strebel, K. (1995) The HIV-1 Vpu protein specifically binds to the CD4 cytoplasmic domain: Implications for the mechanisms of CD4 degradation and viral particle release, *J. Cell. Biochem.*, 187.
20. Bour, S., Schubert, U., and Strebel, K. (1995) The human-immunodeficiency-virus type-1 Vpu protein specifically binds to the cytoplasmic domain of CD4: Implications for the mechanism of degradation, *J. Virol. 69*, 1510−1520.
21. Margottin, F., Benichou, S., Durand, H., Richard, V., Liu, L. X., Gomas, E., and Benarous, R. (1996) Interaction between the cytoplasmic domains of HIV-1 Vpu and CD4: Role of Vpu residues involved in CD4 interaction and in vitro CD4 degradation, *Virology 223*, 381−386.
22. Tiganos, E., Yao, X. J., Friborg, J., Daniel, N., and Cohen, E. A. (1997) Putative α-helical structures in the human immunodeficiency virus type 1 Vpu protein and CD4 are involved in binding and degradation of the CD4 molecule, *J. Virol. 71*, 4452−4460.
23. Margottin, F., Bour, S. P., Durand, H., Selig, L., Benichou, S., Richard, V., Thomas, D., Strebel, K., and Benarous, R. (1998) A novel human WD protein, h-βTrCP, that interacts with HIV-1 Vpu connects CD4 to the ER degradation pathway through an F-box motif, *Mol. Cell 1*, 565−574.
24. Bour, S., and Strebel, K. (2003) The HIV-1 Vpu protein: A multifunctional enhancer of viral particle release, *Microbes Infect. 5*, 1029−1039.
25. Coadou, G., Gharbi-Benarous, J., Megy, S., Bertho, G., Evrard-Todeschi, N., Segeral, E., Benarous, R., and Girault, J. P. (2003) NMR studies of the phosphorylation motif of the HIV-1 protein Vpu bound to the F-box protein beta-TrCP, *Biochemistry 42*, 14741−14751.
26. McCormick-Davis, C., Dalton, S. B., Singh, D. K., and Stephens, E. B. (2000) Comparison of Vpu sequences from diverse geographical isolates of HIV type 1 identifies the presence of highly variable domains, additional invariant amino acids, and a signature sequence motif common to subtype C isolates, *AIDS Res. Hum. Retroviruses 16*, 1089−1095.
27. Wray, V., Kinder, R., Federau, T., Henklein, P., Bechinger, B., and Schubert, U. (1999) Solution structure and orientation of the transmembrane anchor domain of the HIV-1-encoded virus protein U by high-resolution and solid-state NMR spectroscopy, *Biochemistry 38*, 5272−5282.
28. Wray, V., Federau, T., Henklein, P., Klabunde, S., Kunert, O., Schomburg, D., and Schubert, U. (1995) Solution structure of the hydrophilic region of HIV-1 encoded virus protein-U (Vpu) by CD and H-1-NMR spectroscopy, *Int. J. Pept. Protein Res. 45*, 35−43.
29. Kukol, A., and Arkin, I. T. (1999) Vpu transmembrane peptide structure obtained by site-specific Fourier transform infrared dichroism and global molecular dynamics searching, *Biophys. J. 77*, 1594−1601.
30. Federau, T., Schubert, U., Flossdorf, J., Henklein, P., Schomburg, D., and Wray, V. (1996) Solution structure of the cytoplasmic domain of the human immunodeficiency virus type 1 encoded virus protein U (Vpu), *Int. J. Pept. Protein Res. 47*, 297−310.
31. Willbold, D., Hoffmann, S., and Rosch, P. (1997) Secondary structure and tertiary fold of the human immunodeficiency virus protein U (Vpu) cytoplasmic domain in solution, *Eur. J. Biochem. 245*, 581−588.
32. Coadou, G. L., Evrard-Todeschi, N., Gharbi-Benarous, J., Benarous, R., and Girault, J. P. (2002) HIV-1 encoded virus protein U (Vpu) solution structure of the 41−62 hydrophilic region containing the phosphorylated sites Ser(52) and Ser(56), *Int. J. Biol. Macromol. 30*, 23−40.
33. Ma, C., Marassi, F. M., Jones, D. H., Straus, S. K., Bour, S., Strebel, K., Schubert, U., Oblatt-Montal, M., Montal, M., and Opella, S. J. (2002) Expression, purification, and activities of full-length and truncated versions of the integral membrane protein Vpu from HIV-1, *Protein Sci. 11*, 546−547.
34. Park, S. H., Mrse, A. A., Nevzorov, A. A., Mesleh, M. F., Oblatt-Montal, M., Montal, M., and Opella, S. J. (2003) Three-dimensional structure of the channel-forming trans-membrane domain of virus protein "u" (Vpu) from HIV-1, *J. Mol. Biol. 333*, 409−424.
35. Fischer, W. B., Sramala, I., Cordes, F., Angsuthanasombat, C., Sansom, M. S. P., and Watts, A. (2002) Molecular dynamics simulations on up to the first 52 amino acids from HIV-1's Vpu, *Biophys. J. 82*, 534A.
36. Sramala, I., Lemaitre, V., Faraldo-Gomez, J. D., Vincent, S., Watts, A., and Fischer, W. B. (2003) Molecular dynamics simulations on the first two helices of Vpu from HIV-1, *Biophys. J. 84*, 3276−3284.
37. Sun, F. (2003) Molecular dynamics simulation of human immunodeficiency virus protein U (Vpu) in lipid/water Langmuir monolayer, *J. Mol. Model. 9*, 114−123.
38. Cordes, F. S., Kukol, A., Forrest, L. R., Arkin, I. T., Sansom, M. S. P., and Fischer, W. B. (2001) The structure of the HIV-1 Vpu ion channel: Modelling and simulation studies, *Biochim. Biophys. Acta 1512*, 291−298.
39. Cordes, F. S., Tustian, A. D., Sansom, M. S. P., Watts, A., and Fischer, W. B. (2002) Bundles consisting of extended transmembrane segments of Vpu from HIV-1: Computer simulations and conductance measurements, *Biochemistry 41*, 7359−7365.
40. Grice, A. L., Kerr, I. D., and Sansom, M. S. P. (1997) Ion channels formed by HIV-1 Vpu: A modelling and simulation study, *FEBS Lett. 405*, 299−304.
41. Lopez, C. F., Montal, M., Blasie, J. K., Klein, M. L., and Moore, P. B. (2002) Molecular dynamics investigation of membrane-bound bundles of the channel-forming transmembrane domain of viral protein U from the human immunodeficiency virus HIV-1, *Biophys. J. 83*, 1259−1267.
42. Moore, P. B., Zhong, Q. F., Husslein, T., and Klein, M. L. (1998) Simulation of the HIV-1 Vpu transmembrane domain as a pentameric bundle, *FEBS Lett. 431*, 143−148.
43. Montal, M. (2003) Structure−function correlates of Vpu, a membrane protein of HIV-1, *FEBS Lett. 552*, 47−53.
44. Fischer, W. B. (2003) Vpu from HIV-1 on an atomic scale: Experiments and computer simulations, *FEBS Lett. 552*, 39−46.
45. Park, S. H., and Opella, S. J. (2005) Tilt angle of a trans-membrane helix is determined by hydrophobic mismatch, *J. Mol. Biol. 350*, 310−318.
46. Henklein, P., Kinder, R., Schubert, U., and Bechinger, B. (2000) Membrane interactions and alignment of structures within the HIV-1 Vpu cytoplasmic domain: Effect of phosphorylation of serines 52 and 56, *FEBS Lett. 482*, 220−224.
47. Gonzalez, M. E., and Carrasco, L. (2003) Viroporins, *FEBS Lett. 552*, 28−34.
48. Guinea, R., and Carrasco, L. (1994) Concanamycin-A blocks influenza-virus entry into vells under acidic conditions, *FEBS Lett. 349*, 327−330.
49. Mould, J. A., Drury, J. E., Frings, S. M., Kaupp, U. B., Pekosz, A., Lamb, R. A., and Pinto, L. H. (2000) Permeation and activation of the M-2 ion channel of influenza A virus, *J. Biol. Chem. 275*, 31038−31050.
50. Pinto, L. H., Holsinger, L. J., and Lamb, R. A. (1992) Influenza-virus M2 protein has ion channel activity, *Cell 69*, 517−528.
51. Pinto, L. H., Dieckmann, G. R., Gandhi, C. S., Papworth, C. G., Braman, J., Shaughnessy, M. A., Lear, J. D., Lamb, R. A., and DeGrado, W. F. (1997) A functionally defined model for the M-2 proton channel of influenza A virus suggests a mechanism for its ion selectivity, *Proc. Natl. Acad. Sci. U.S.A. 94*, 11301−11306.
52. Griffin, S. D. C., Beales, L. P., Clarke, D. S., Worsfold, O., Evans, S. D., Jaeger, J., Harris, M. P. G., and Rowlands, D. J. (2003) The p7 protein of hepatitis C virus forms an ion channel that is blocked by the antiviral drug, Amantadine, *FEBS Lett. 535*, 34−38.
53. Carrere-Kremer, S., Montpellier-Pala, C., Cocquerel, L., Wychowski, C., Penin, F., and Dubuisson, J. (2002) Subcellular localization and topology of the p7 polypeptide of hepatitis C virus, *J. Virol. 76*, 3720−3730.

54. Gonzalez, M. E., and Carrasco, L. (1998) The human immunodeficiency virus type 1 Vpu protein enhances membrane permeability, *Biochemistry 37*, 13710−13719.
55. Tian, C. L., Gao, P. F., Pinto, L. H., Lamb, R. A., and Cross, T. A. (2003) Initial structural and dynamic characterization of the M2 protein transmembrane and amphipathic helices in lipid bilayers, *Protein Sci. 12*, 2597−2605.
56. Nishimura, K., Kim, S. G., Zhang, L., and Cross, T. A. (2002) The closed state of a H^+ channel helical bundle combining precise orientational and distance restraints from solid-state NMR-1, *Biochemistry 41*, 13170−13177.
57. Marassi, F. M., and Crowell, K. J. (2003) Hydration-optimized oriented phospholipid bilayer samples for solid-state NMR structural studies of membrane proteins, *J. Magn. Reson. 161*, 64−69.
58. Bielecki, A., and Burum, D. P. (1995) Temperature-dependence of Pb-207 MAS spectra of solid lead nitrate: An accurate, sensitive thermometer for variable-temperature MAS, *J. Magn. Reson., Ser. A 116*, 215−220.
59. Silvius, J. R. (1982) in *Lipid−Protein Interactions*, John Wiley & Sons, New York.
60. Zhou, Z., Sayer, B. G., Hughes, D. W., Stark, R. E., and Epand, R. M. (1999) Studies of phospholipid hydration by high-resolution magic-angle spinning nuclear magnetic resonance, *Biophys. J. 76*, 387−399.
61. Pines, A., Gibby, M. G., and Waugh, J. S. (1973) Proton-enhanced NMR of dilute spins in solids, *J. Chem. Phys. 59*, 569−590.
62. Morcombe, C. R., Gaponenko, V., Byrd, R. A., and Zilm, K. W. (2004) Diluting abundant spins by isotope edited radio frequency field assisted diffusion, *J. Am. Chem. Soc. 126*, 7196−7197.
63. Takegoshi, K., Nakamura, S., and Terao, T. (2001) ^{13}C-^{1}H dipolar-assisted rotational resonance in magic-angle spinning NMR, *Chem. Phys. Lett. 344*, 631−637.
64. Baldus, M., Petkova, A. T., Herzfeld, J., and Griffin, R. G. (1998) Cross polarization in the tilted frame: Assignment and spectral simplification in heteronuclear spin systems, *Mol. Phys. 95*, 1197−1207.
65. Petkova, A. T., Baldus, M., Belenky, M., Hong, M., Griffin, R. G., and Herzfeld, J. (2003) Backbone and side chain assignment strategies for multiply labeled membrane peptides and proteins in the solid state, *J. Magn. Reson. 160*, 1−12.
66. Bennett, A. E., Rienstra, C. M., Auger, M., Lakshmi, K. V., and Griffin, R. G. (1995) Heteronuclear decoupling in rotating solids, *J. Chem. Phys. 103*, 6951−6958.
67. Long, H. W., and Tycko, R. (1998) Biopolymer conformational distributions from solid-state NMR: α-Helix and 3(10)-helix contents of a helical peptide, *J. Am. Chem. Soc. 120*, 7039−7048.
68. Delaglio, F., Grzesiek, S., Vuister, G. W., Zhu, G., Pfeifer, J., and Bax, A. (1995) NMRpipe: A multidimensional spectral processing system based on Unix pipes, *J. Biomol. NMR 6*, 277−293.
69. Cornilescu, G., Delaglio, F., and Bax, A. (1999) Protein backbone angle restraints from searching a database for chemical shift and sequence homology, *J. Biomol. NMR 13*, 289−302.
70. Jones, D. H., Ball, E. H., Sharpe, S., Barber, K. R., and Grant, C. W. M. (2000) Expression and membrane assembly of a transmembrane region from Neu, *Biochemistry 39*, 1870−1878.
71. Grisshammer, R., and Tate, C. G. (1995) Overexpression of integral membrane-proteins for structural studies, *Q. Rev. Biophys. 28*, 315−422.
72. Tamm, L. K., and Seelig, J. (1983) Lipid solvation of cytochrome-C oxidase: Deuterium, N-14, and P-31 nuclear magnetic-resonance studies on the phosphocholine head group and on cis-unsaturated fatty acyl chains, *Biochemistry 22*, 1474−1483.
73. Scherer, P. G., and Seelig, J. (1989) Electric charge effects on phospholipid headgroups: Phosphatidylcholine in mixtures with cationic and anionic amphiphiles, *Biochemistry 28*, 7720−7728.
74. Fares, C., Qian, J., and Davis, J. H. (2005) Magic angle spinning and static oriented sample NMR studies of the relaxation in the rotating frame of membrane peptides, *J. Chem. Phys. 122*.
75. Bodner, M. L., Gabrys, C. M., Parkanzky, P. D., Yang, J., Duskin, C. A., and Weliky, D. P. (2004) Temperature dependence and resonance assignment of C-13 NMR spectra of selectively and uniformly labeled fusion peptides associated with membranes, *Magn. Reson. Chem. 42*, 187−194.
76. Lewis, B. A., Harbison, G. S., Herzfeld, J., and Griffin, R. G. (1985) NMR structural analysis of a membrane protein: Bacteriorhodopsin peptide backbone orientation and motion, *Biochemistry 24*, 4671−4679.
77. Hu, W., Lazo, N. D., and Cross, T. A. (1995) Tryptophan dynamics and structural refinement in a lipid bilayer environment: Solid-state NMR of the gramicidin channel, *Biochemistry 34*, 14138−14146.
78. Wishart, D. S., Bigam, C. G., Holm, A., Hodges, R. S., and Sykes, B. D. (1995) H-1, C-13 and N-15 random coil NMR chemical-shifts of the common amino acids. 1. Investigations of nearest-neighbor effects, *J. Biomol. NMR 5*, 67−81.
79. Saito, H. (1986) Conformation-dependent ^{13}C chemical shifts: A new means of conformational characterization as obtained by high-resolution solid-state ^{13}C NMR, *Magn. Reson. Chem. 24*, 835−852.
80. Spera, S., and Bax, A. (1991) Empirical correlation between protein backbone conformation and Cα and Cβ ^{13}C nuclear magnetic resonance chemical shifts, *J. Am. Chem. Soc. 113*, 5490−5492.
81. Petkova, A. T., Ishii, Y., Balbach, J. J., Antzutkin, O. N., Leapman, R. D., Delaglio, F., and Tycko, R. (2002) A structural model for Alzheimer's β-amyloid fibrils based on experimental constraints from solid-state NMR, *Proc. Natl. Acad. Sci. U.S.A. 99*, 16742−16747.
82. Sharpe, S., Kessler, N., Anglister, J. A., Yau, W. M., and Tycko, R. (2004) Solid-state NMR yields structural constraints on the V3 loop from HIV-1 Gp120 bound to the 447−52D antibody Fv fragment, *J. Am. Chem. Soc. 126*, 4979−4990.
83. Prosser, R. S., Davis, J. H., Mayer, C., Weisz, K., and Kothe, G. (1992) Deuterium NMR Relaxation Studies of Peptide-Lipid Interactions, *Biochemistry 31*, 9355−9363.
84. Prosser, R. S., and Davis, J. H. (1994) Dynamics of an integral membrane peptide: A deuterium NMR relaxation study of Gramicidin, *Biophys. J. 66*, 1429−1440.
85. Datema, K. P., Pauls, K. P., and Bloom, M. (1986) Deuterium nuclear-magnetic-resonance investigation of the exchangeable sites on Gramicidin-A and Gramicidin-S in multilamellar vesicles of dipalmitoylphosphatidylcholine, *Biochemistry 25*, 3796−3803.
86. Macdonald, P. M., and Seelig, J. (1988) Dynamic properties of gramicidin-A in phospholipid membranes, *Biochemistry 27*, 2357−2364.
87. Herzfeld, J., and Berger, A. E. (1980) Sideband intensities in NMR spectra of samples spinning at the magic angle, *J. Chem. Phys. 73*, 6021−6030.
88. Teng, Q., and Cross, T. A. (1989) The *in situ* determination of the N-15 chemical-shift tensor orientation in a polypeptide, *J. Magn. Reson. 85*, 439−447.
89. Bai, Y. W., Milne, J. S., Mayne, L., and Englander, S. W. (1993) Primary structure effects on peptide group hydrogen-exchange, *Proteins 17*, 75−86.
90. Tatulian, S. A., Cortes, D. M., and Perozo, E. (1998) Structural dynamics of the *Streptomyces lividans* K^+ channel (SKC1): Secondary structure characterization from FTIR spectroscopy, *FEBS Lett. 423*, 205−212.
91. Becker, C. F. W., Oblatt-Montal, M., Kochendoerfer, G. G., and Montal, M. (2004) Chemical synthesis and single channel properties of tetrameric and pentameric TASPs (template-assembled synthetic proteins) derived from the transmembrane domain of HIV virus protein u (Vpu), *J. Biol. Chem. 279*, 17483−17489.
92. Petkova, A. T., Buntkowsky, G., Dyda, F., Leapman, R. D., Yau, W. M., and Tycko, R. (2004) Solid-state NMR reveals a pH-dependent antiparallel β-sheet registry in fibrils formed by a β-amyloid peptide, *J. Mol. Biol. 335*, 247−260.
93. Pauls, K. P., Mackay, A. L., Soderman, O., Bloom, M., Tanjea, A. K., and Hodges, R. S. (1985) Dynamic properties of the backbone of an integral membrane polypeptide measured by H-2-NMR, *Eur. Biophys. J. 12*, 1−11.
94. Sharpe, S., Barber, K. R., Grant, C. W. M., Goodyear, D., and Morrow, M. R. (2002) Organization of model helical peptides in lipid bilayers: Insight into the behavior of single-span protein transmembrane domains, *Biophys. J. 83*, 345−358.
95. Sharpe, S., Barber, K. R., and Grant, C. W. M. (2002) Evidence of a tendency to self-association of the transmembrane domain of ErbB-2 in fluid phospholipid bilayers, *Biochemistry 41*, 2341−2352.
96. Spooner, P. J. R., Friesen, R. H. E., Knol, J., Poolman, B., and Watts, A. (2000) Rotational mobility and orientational stability of a transport protein in lipid membranes, *Biophys. J. 79*, 756−766.
97. Wishart, D. S., and Case, D. A. (2001) Use of chemical shifts in macromolecular structure determination, *Methods Enzymol. 338*, 3−34.

98. Kim, S., Jeon, T.-J., Oberai, A., Yang, D., Schmidt, J. J., and Bowie, J. U. (2005) Transmembrane glycine zippers: Physiological and pathological roles in membrane proteins, *Proc. Natl. Acad. Sci. U.S.A. 102*, 14278−14283.
99. Ozdirekcan, S., Rijkers, D. T. S., Liskamp, R. M. J., and Killian, J. A. (2005) Influence of flanking residues on tilt and rotation angles of transmembrane peptides in lipid bilayers. A solid-state H-2 NMR study, *Biochemistry 44*, 1004−1012.
100. Canutescu, A. A., Shelenkov, A. A., and Dunbrack, R. L. (2003) A graph-theory algorithm for rapid protein side-chain prediction, *Protein Sci. 12*, 2001−2014.
101. Wiener, M. C., and White, S. H. (1992) Structure of a fluid dioleoylphosphatidylcholine bilayer determined by joint refinement of X-ray and neutron-diffraction data. 3. Complete structure, *Biophys. J. 61*, 434−447.
102. Koradi, R., Billeter, M., and Wuthrich, K. (1996) MOLMOL: A program for display and analysis of macromolecular structures, *J. Mol. Graphics 14*, 51−55.

BI051766K